UNIVERSITÉ DE GENÈVE

FACULTÉ DES SCIENCES

FUTURE CIRCULAR COLLIDER

On the

Phenomenology of Dirac and Majorana type Heavy Neutral Leptons and their searches at the FCC-ee

Tanishq Sharma
University of Geneva

CERN-THESIS-2022-089
12/07/2022

Supervised by:

Anna Sfyrla
University of Geneva

Francesco Riva
University of Geneva

July 2022

Geneva, Switzerland

Abstract

Neutrinos in the Standard Model are massless particles, however neutrino oscillation experiments have demonstrated that neutrinos have masses. Beyond the Standard Model theories exist to introduce neutrino mass mechanisms. Some of these models do so by postulating the existence of additional particles, the heavy neutral leptons (HNLs). These particles can be of Dirac or Majorana type based on the specific model. In this thesis, theoretical computations show possible kinematical variables of final state particles that can provide discrimination between the Dirac vs Majorana nature of the HNLs and experimental simulations and analysis show the possibility of such discrimination within the context of their possible discovery at the FCC-ee experiment at CERN.

Table of Contents

Introduction 3

Section 1: Theory

Chapter 1: Standard Model and the need for BSM theories 5

Chapter 2: Neutrino mass mechanisms 16

Chapter 3: Theoretical Computations of the HNL 22

Section 2: Experiment

Chapter 4: Introduction to FCC-ee and the FCC Framework 37

Chapter 5: HNL Simulations and Analysis 42

Chapter 6: Summary and Conclusion 62

Appendices

Appendix A 65

Appendix B 75

References 76

Introduction

The Standard Model of Particle physics is the primary theory of fundamental particles and interactions, and has shown excellent agreements with experiments. Nevertheless, it leaves many questions unanswered, for instance, the nature of dark matter, gravity, or the origin of neutrino masses. In such a scenario, Beyond the Standard Model physics comes in to try and hypothesize the answers to these open questions.

One such important question, as mentioned above, is that of the origin of neutrino masses. Standard model predicts neutrinos to be massless particles, however, observations of neutrino oscillations suggest that neutrinos have masses. It then becomes important to explore models that can provide mechanisms for generating neutrino masses in a way that is consistent with the Standard Model. There exist many such models, and a few of these models achieve neutrino mass mechanisms by introducing sterile heavy neutrino mass eigenstates, or heavy neutral leptons. Based on the specific model, the heavy neutral lepton can be a Dirac particle (one that participates in lepton number conserving processes) or a Majorana particle (one that participates in lepton number conserving and violating processes).

In this project, I begin with exploring all the necessary theoretical prerequisites building up to the Type I and Inverse seesaw models. The heavy neutral leptons, as proposed in these models are then studied by performing helicity amplitude computations pertaining to the leptonic decay modes of the heavy neutral leptons. The amplitudes are then used for computation of differential decay width with respect to an angular variable (θ_{ee}), the angle between the final state electron and positron. It is shown that this variable is able to provide for some amount of discrimination between the Dirac and Majorana type HNLs.

The next part of the project concerns the generation of events simulating the production and leptonic channel decay of the heavy neutral leptons in the center of mass energy of ~ 91 GeV based on the proposed Tera Z Run phase of the Future Circular Collider-ee(FCC-ee) experiment, which is a proposed next generation collider at CERN. The events undergo detector simulation to obtain final samples, which are then analyzed within the FCC-ee framework. The analysis shows that the angular variable (θ_{ee}) does provide discrimination between the Dirac and Majorana type heavy neutral leptons(HNLs), and that if such a particle is indeed observed at the FCC-ee, it should be possible to comment on its nature to some extent.

As a result, the theoretical computations and experimental simulations and analysis show complementarity in distinguishing between the Dirac vs Majorana nature of a heavy neutral lepton, should it exist and is discovered, in a future experiment.

The thesis will be structured as follows: In the first chapter, I will provide an overview of the mass mechanisms in the Standard Model to understand why neutrinos of the SM are massless. I will also discuss the requirement of neutrino masses imposed by neutrino oscillation experiments. In the second chapter, I will explore the Type I seesaw and Inverse seesaw models that gives rise to Majorana and Dirac type HNLs respectively. Chapter 3 will comprise of the theoretical computations done in this project. In the fourth chapter, I will provide an overview of the FCC-ee and the FCC framework. In the fifth chapter, I will go into the details of the experimental analysis done in this project.

Chapter 1: Standard Model and the need for BSM theories

The Standard model is a very successful and self consistent quantum field theory that explains a lot of the elementary physics phenomena at currently accessible energies. The Standard model provides a list of fundamental particles and their properties such as rest mass, electric charge, color charge, particle type, etc., are often deduced experimentally. In the quantum field theory prescription, these particles correspond to the excitations of their respective fields that can be created using creation operators and annihilated using annihilation operators. Any field theory can be characterized by its Lagrangian that contains kinetic terms, mass terms and interaction terms. A more quantitative review of this description can be found in any standard quantum field theory textbook, however, the focus here will now shift to understanding the mass terms in a Lagrangian.

Mass terms in QED Lagrangian

A very important symmetry in physics is gauge symmetry. The idea that physics remains the same for observers in different reference frames is paramount to being able to deduce universal laws of nature in the first place. In quantum field theory, transformations of any kind are represented by members of a Group G where the group G acts as a representation of the symmetry itself. Mathematically, this means that a transformation that takes a certain quantity ϕ^i to ϕ^j happens such that:

$\phi^j = g^j{}_i \phi^i$ where $g \in G$

We now take a look at a very simple theory that will effectively display the above mentioned concepts for further use. Consider a complex scalar field ϕ where $\phi = \phi_1 + i\phi_2$, where ϕ_1 and ϕ_2 denote real fields. The action of this theory would be given as

$$S = \int d^4x \ \ \partial_\mu \phi \partial^\mu \phi^* + m^2 \phi^* \phi$$

Action, which is always a dimensionless invariant, is the time integral of Lagrangian, which is itself a space integral of Lagrangian density. From here onwards, the term Lagrangian will be used to denote both the Lagrangian and the Lagrangian density. Hence, we have a Lagrangian of $\partial_\mu \phi \partial^\mu \phi^* + m^2 \phi^* \phi$ for the complex scalar theory.

Consider a transformation such that $\phi \rightarrow e^{i\theta}\phi$. The conjugate of the expression is $\phi^* \rightarrow e^{-i\theta}\phi^*$. We have the rules of transformation for this theory and applying it to the Lagrangian yields the following:

$$\partial_\mu e^{i\theta}\phi \partial^\mu e^{-i\theta}\phi^* + e^{i\theta}e^{-i\theta}m^2\phi^*\phi = \ \partial_\mu \phi \partial^\mu \phi^* + m^2 \phi^* \phi$$

As shown, this transformation leaves the Lagrangian, and consequently the action unchanged. What we have seen here is that the group $U(1)$, a group denoting unitary transformations of degree 1, is a global symmetry of our theory.

We have now looked at a very simplistic example that will allow us to move further into understanding the requirements for mass terms of real particles in the Standard Model. Before moving onto that though, the concepts of spin, helicity and chirality needs to be understood. The concept of spin is such that, consider a particle that has an angular momentum without any rotations, this angular momentum must thus originate from some intrinsic property of the particle, which is its spin. The spin can be characterized using a vector by visualizing a system such that for a 3d space, for angular momentum in anticlockwise direction for an observe located at any point on positive z-axis, the positive

direction of z-axis is itself the spin vector. Spin is an axial vector, i.e. a vector that doesn't change sign under a parity transformation.

Consider a particle with spin $\boldsymbol{s}$ moving with momentum $\boldsymbol{p}$. The sign of the dot product $\boldsymbol{s}.\boldsymbol{p}$ could be positive or negative, where a positive sign characterizes positive or right handed helicity, and a negative sign characterizes negative or left handed helicity. It is important to note that helicity is not an invariant for a massive particle as a massive particle could be boosted (Lorentz transformation pertaining to speed) to a frame such that the direction of $\boldsymbol{p}$ could be flipped. However, for a massless particle, travelling at the speed of light, no such transformation exists and therefore helicity for a massless particle is invariant under any Lorentz transformations.

Lorentz transformations include boosts and rotations. When coupled with translations, they form the Poincare transformations characterized by the Poincare group. The concept of chirality is very abstract and it becomes hard to visualize it, however, mathematically the chirality of a particle is whether it transforms in a left handed or a right handed representation of the Poincare group. For a massless particle, helicity and chirality are the same, whereas for massive particles, they are not. Electrons, for instance, are Dirac particles which are denoted by a Dirac spinor ψ. The left handed transformation of the Poincare group is given by $\frac{1}{2}(1-\gamma^5)$ and the right handed transformation is given by $\frac{1}{2}(1+\gamma^5)$. A left chiral electron is given as $\psi_L = \frac{1}{2}(1-\gamma^5)\psi$.

We have now looked at concepts, at least qualitatively, that will allow us to look at mass terms quantitatively. To look at mass terms, we will turn our focus to quantum electrodynamics particles. The Lagrangian of QED is given as:

$$\mathcal{L} = \bar{\psi}(i\partial\!\!\!/ - m)\psi - \frac{1}{4}F^{\mu\nu}F_{\mu\nu}$$

The Dirac spinor ψ can be written as $\psi_L + \psi_R$ and its adjoint $\bar{\psi}$ is defined as $\psi^\dagger\gamma^0$.

The mass term $m\bar{\psi}\psi$ is given as shown below:

$$m\bar{\psi}\psi = m(\overline{\psi_L}\psi_L + \overline{\psi_L}\psi_R + \overline{\psi_R}\psi_L + \overline{\psi_R}\psi_R)$$

$$= m(\bar{\psi}P_R P_L\psi + \bar{\psi}P_R P_R\psi + \bar{\psi}P_L P_L\psi + \bar{\psi}P_L P_R\psi)$$

$P_L P_R = P_R P_L = 0$ and hence $m\bar{\psi}\psi$ reduces to $m(\overline{\psi_L}\psi_R + \overline{\psi_R}\psi_L)$.

Furthermore, the symmetry of QED is that of $U(1)_{em}$ group and transformations under $U(1)_{em}$ too leave the Lagrangian (including the mass term) invariant. The $U(1)_{em}$ transformations can be global, i.e. where $\psi \to e^{i\alpha}\psi$ or local, i.e. $\psi \to e^{i\alpha(x)}\psi$. However, in case of local gauge symmetry, the photon field becomes relevant as regular derivatives are replaced by covariant derivatives. We now turn our attention to the Standard Model.

Mass terms in SM Lagrangian

The symmetry group of the standard model is given by $SU(3)_q * SU(2)_L * U(1)_Y$. The $SU(3)_q$ corresponds to the framework of quantum chromodynamics and we will leave it aside for the purposes of this thesis. The $SU(2)_L * U(1)_Y$ denotes the electroweak part of the standard model. Before taking a look at the group pertaining to the electroweak interaction, it is a good idea to qualitatively understand the historical development of neutrino physics to understand the motivation behind the structure of the electroweak group. An interested reader is encouraged to look at [1] for a more detailed overview.

Neutrinos do not make up the everyday matter. The proposition of their existence arose as a need to explain the beta decay spectrum. The decay of a neutron to produce a proton and a beta particle (electron) was expected to give the emitted beta particle a fixed amount of energy, however, when the energy of these beta particles was measured, a spectrum was observed that ended at the expected energy point. Today we understand that this decay process also produces an antineutrino that takes away a variable amount of energy leaving us with an energy spectrum for the beta particles. An important point to note here is that this is a weak interaction process, hence electrons take part in weak interactions, and hence they should have some 'weak interactions charge'. Neutrinos do not have an electric charge (due to charge conservation) and hence they do not take part in QED interactions but rather only in weak interactions. The fact that electrons take part in QED and weak interactions is a motivation for wanting to bring the two interactions into a unified framework of electroweak interactions.

The next historical development in the field that we need to understand is that of the discovery of parity violation in weak interactions. An experiment of importance is described in [2]. The full explanation of parity violating interactions is beyond the scope of this thesis, hence we will focus on some key observations that have been made experimentally in the field.

1. Weak interactions constitute of charged current and neutral current interactions
2. Charged current interactions only involve particles with left handed chirality
3. Neutral current interactions can involve particles of both chirality but usually involves a slight bias towards left handed chirality

4. There has been no observation of neutrinos with a right handed chirality

These observations highlight the importance and structuring of the 'weak interactions charge' mentioned above, which is actually called the weak hypercharge. In the weak interactions, the left handed electron and the left handed neutrino have the same hypercharge and are paired into a doublet (as are their charge conjugated anti-particles) as: $l_L = \begin{pmatrix} \nu_{eL} \\ e_L \end{pmatrix}$ which has a weak hypercharge of -1. The right handed electrons have a different hypercharge and they exist as singlets as e_R with a weak hypercharge of -2. The existence of right handed neutrinos is not known, and if they do exist, their hypercharge would be 0 as they do not participate in weak interactions. This entire prescription covers the next generation of leptons too, i.e. μ and τ.

We now have 2 out 4 components that make up the Standard Model's leptonic mass terms. For the next two terms, we need to understand the physics of the Higgs Field. Its detailed review is outside the scope of this thesis, however due to its importance, I will attempt to provide a heuristic explanation of the topic that should enable the reader to understand the Standard Model mass terms.

There are two main problems with the electroweak interactions briefly described above. The first is that massive gauge bosons break local gauge invariance of a theory, however, the gauge bosons of weak interactions (W^-, W^+ and Z) are massive. The second is that we have put left handed particles in doublets, that transform as doublets under the $SU(2)$ group whereas the right handed particles which are singlets, transform as singlets under the $SU(2)$ group. To transform as a doublet under the $SU(2)$ group means to undergo transform as: $\phi \rightarrow e^{-\frac{i}{2}\omega^i \sigma_i}\phi$ where σ_i are the Pauli matrices. To transform as a singlet under the $SU(2)$

group means to stay invariant. These transformations do not cancel one another and thus the gauge invariance, as was shown above for the QED Lagrangian mass terms, does not exist here. The introduction of the Higgs Field solves both these issues, and we will be focusing on how the second issue is solved.

The Higgs field is composed of a complex scalar doublet. To understand this, firstly consider a real scalar field ϕ with a kinetic term, $\partial^\mu\phi\partial_\mu\phi$, and a potential term, $\frac{1}{2}\mu^2\phi^2 + \frac{1}{4}\lambda\phi^4$. The quadratic term can be thought of as the mass term with μ being the mass, and the quartic term can be thought of as the self interaction term. For this field to have a finite minima, $\lambda > 0$. However, the mass term has no such constraints. If we take a mass term whereby $\mu^2 < 0$, we end up with a potential that does not have its minima at 0, but rather has two minima at $\pm\sqrt{\frac{-\mu^2}{\lambda}}$.

If we extend such an argument to a complex scalar field $\phi = \phi_1 + i\phi_2$, the minima of such a field would not be at 0, but rather be a circle in the complex plane, giving the well known 'Mexican-hat potential'. The Higgs field is a doublet of two such complex scalar fields. What happens in such a field is that at $\phi = 0$, the vacuum expectation value is non zero. Furthermore, since the potential is rotationally symmetric, the circle on the complex plane that corresponds to the minima of the field, denotes an infinite number of degenerate vacuum states. Choosing a particular vacuum state breaks the symmetry of the system and this process is known as the Spontaneous Symmetry Breaking of the Electroweak Symmetry. The Higgs doublet, which is given as $\phi = \begin{pmatrix}\phi^+\\ \phi^0\end{pmatrix} = \begin{pmatrix}\phi_1 + i\phi_2\\ \phi_3 + i\phi_4\end{pmatrix}$, after the spontaneous symmetry breaking can be written as $\phi = \frac{1}{\sqrt{2}}\begin{pmatrix}0\\ v\end{pmatrix}$, where v is the vacuum expectation value.

This choice of vacuum state can be made without loss of generalization and expanding about this state yields $\phi = \frac{1}{\sqrt{2}}\begin{pmatrix} 0 \\ v + h(x) \end{pmatrix}$. This $h(x)$ is the neutral scalar observed that is a remnant of the Higgs doublet, known as the Higgs Boson Particle.

The SM Lagrangian has Yukawa terms, which are coupling terms between Scalar fields and Dirac fields. Consider the term: $\mathcal{L}_{int} = -Y_e\left(\overline{l_L}\phi e_R + \overline{e_R\phi} l_L\right)$, where Y_e is the Yukawa coupling, l_L is the left handed lepton doublet, ϕ is the Higgs doublet and e_R is the right handed electron singlet. This term stays invariant under the group transformation. Expanding out this expression gives:

$$\mathcal{L}_{int} = -\frac{Y_e v}{\sqrt{2}}(\bar{e_L}e_R + \overline{e_R}e_L) - \frac{Y_e}{\sqrt{2}}(\bar{e_L}e_R + \overline{e_R}e_L)h$$

We then choose $\frac{Y_e v}{\sqrt{2}} = m_e$, and then the above expression can be written as:

$$\mathcal{L}_{int} = -m_e\bar{e}e - \frac{m_e}{v}\bar{e}e$$

The first term corresponds to the mass of the electron, and the second term corresponds to the coupling between electron and Higgs boson. To physically interpret the idea that the coupling of electron with the Higgs field gives electron its mass, it is worth remembering that the weak hypercharge of the left handed electron is different from the weak hypercharge of the right handed electron. The Higgs field can be thought as an infinite source and sink of weak hypercharge and therefore it can interact with a left handed electron taking away a unit of hypercharge and turning it into a right handed electron, and vice versa. This interaction slows down the electron. It is useful to draw a crude analogy of this process with that of photons originating from the Sun. A photon requires ~ 8 minutes to reach the Earth

from the surface of the Sun, but it requires time that is orders of magnitudes larger for it to reach the surface of the Sun from the center of the Sun. This is due to the fact that photons inside the Sun are constantly interacting with the plasma. Similarly, it can be thought of the fermion being 'slowed down' due to its interaction with the Higgs field, effectively making it a massive particle. The coupling of a fermion would dictate how much the particle is 'slowed down', and therefore the mass of a fermion is directly proportional to its Yukawa coupling with the Higgs field. This concludes the section on mass terms in the SM and we are now ready to discuss neutrino masses.

Neutrino masses

From the Standard Model Lagrangian, we see clearly that there is no coupling between neutrinos and the Higgs field. As a result, a direct prediction of the Standard Model is that neutrinos are massless. However, experimental observations have shown neutrinos have masses. These experiments have observed the phenomena of neutrino oscillations which we will now explore. The phenomena of neutrino oscillations is, like previous concepts, quite thorough with decades of research work gone into it and therefore I will once again be taking a heuristic approach in laying it out in this section.

The nuclear fusion reactions that happen in our Sun and the rates of such reactions are well understood and computed respectively. A very large number of electron neutrinos are produced through these processes, so much so that it becomes possible to detect them despite the fact that they only interact weakly. By knowing the estimated flux of neutrinos passing through a detector and knowing the weak coupling constant, it is possible to estimate the number of neutrinos that should be observed. This experiment resulted in

unpredicted results, in particular, the number of electron neutrinos observed was always less than the estimated number. The deficit approximately ranged from one half to two thirds. This is known as the Solar Neutrino Problem.

The solution to this problem lies in how one thinks about a particle in the first place. When we conceptualize a particle, we think of it as an entity that moves around and interacts (including scattering and decay processes) as an individual entity. It is this simple notion which needs to be abandoned in understanding the nature of neutrinos. In particular, for neutrinos, the entities which interact are not the same entities which move around, or propagate. In formal terms, neutrinos interact as flavor eigenstates, which are states we generally think of when we refer to neutrinos: $v_{e,\mu,\tau}$. However, neutrinos propagate as mass eigenstates, denoted as: $v_{1,2,3}$. Each of the flavor eigenstates can be written as a linear combination of the mass eigenstates and each of the mass eigenstates can be written as a linear combination of the flavor eigenstates. In particular,

$$|v_\alpha\rangle = \sum_i U_{\alpha i} \, |v_i\rangle$$

$$|v_i\rangle = \sum_\alpha U^*_{\alpha i} \, |v_\alpha\rangle$$

Where $U_{\alpha i}$ is the PMNS matrix which is a complex matrix that contains the mixing terms between the individual flavor and mass eigenstates, v_α are the flavor eigenstates with $\alpha = e, \mu$ or τ and v_i are the mass eigenstates with $i = 1, 2$ or 3. The propagation frequency of each of the mass eigenstate is distinct and this results in the interference of the mass eigenstates to oscillate. A state which is a superposition of these mass eigenstates would as a result

oscillate too. A more mathematical description of the process of neutrino oscillations can be found in [3].

The phenomena of neutrino oscillations has been well studied in many different experiments. The study of this phenomena is not able to deduce the mass of the mass eigenstates but rather the mass difference between pairs of mass eigenstates. As a result, at least two neutrino mass terms are required to be additionally added to the Standard Model Lagrangian.

The physics of Standard Model and Neutrino Physics are very rich fields in physics and a short thesis chapter can never do justice to their complexity. However, I hope this chapter is able to clearly demonstrate that the Standard Model of Particle Physics predicts neutrinos to be massless particles, however the experimental observations of neutrino oscillations require the existence of massive neutrinos. This lays the foundation that necessitates the exploration of Beyond the Standard Model Physics to explain masses of neutrinos that are compatible with Standard Model Physics. This concludes the 1st chapter of the thesis and the next chapter will focus on two types of BSM models that allow for neutrino masses.

Chapter 2: Neutrino mass mechanisms

In the last chapter, it was shown that mass terms require left and right handed states of a given particle. For neutrinos, only the left handed state has been observed suggesting neutrinos are massless particles in the Standard Model. However, the observations of the phenomena of neutrino oscillations suggests that neutrinos do have masses (at least for 2 out of 3 generations). In this chapter we will look at a couple of specific BSM models that allow for neutrino mass terms that will be the focus of the rest of the thesis.

From the simplicity standard point, one may question what is the simplest mechanism that introduces neutrino mass terms? The simplest mechanism would be to just introduce a right handed neutrino state v_R, set its weak hypercharge to 0, thereby making it a sterile particle, i.e. one that does not have any possible interactions but still allowing us to write mass terms of the form $m\overline{v_L}v_R + m\overline{v_R}v_L$. However, if it was that simple, my thesis would be ending here. The problem with such a mass term is that of scales. The smallest mass for a Standard Model particle is that of an electron, which is approximately 0.5 MeV. The upper bound on neutrino masses is approximately 0.1 eV. In such a case, one wonders why the Yukawa coupling of a neutrino is 6-7 orders of magnitude smaller (but not 0) than the smallest Yukawa coupling in the Standard Model (which is of the electron).

It is here where it becomes worthwhile to look at models that not only introduce neutrino mass terms, but also explain the smallness of the neutrino's mass term. One class of theories such theories are called seesaw models. In some of these models, heavy sterile neutrino mass eigenstates are introduced and their 'heaviness' leads to the 'lightness' of the regular neutrinos. In this chapter, we will be looking at two types of seesaw models that introduce two types heavy neutrino mass eigenstates or heavy neutral leptons which will be the focus

of the rest of this thesis. However, before that, we will take a slight detour to look at the concept of a Majorana particle.

Majorana Fermions

In the last chapter, we saw that the Dirac spinor ψ is a sum of the left and right handed fields $\psi_L + \psi_R$. In explicit 4 component form, a Dirac spinor is given as $\psi = \begin{bmatrix} \psi_L \\ \psi_R \end{bmatrix}$ where the top and bottom terms are both 2 component terms. Consider an operator $\boldsymbol{C}$, which acts on spinors such that $\boldsymbol{C}\bar{\psi}^T = \psi^c = \begin{bmatrix} -i\sigma^2{\psi^*}_R \\ i\sigma^2{\psi^*}_L \end{bmatrix}$. This operator, which is called the charge conjugation operator, takes a field and flips its charge and its 'handed-ness'. For instance, applying this operator on a left handed electron spinor would give a right handed positron spinor. This is not a transformation of chirality as left handed particle and right handed anti-particles are both left chiral states.

Now consider a case such that $\psi^c = \psi$. This condition is forbidden for a charged lepton because this would mean the charge of an electron and a positron is the same. More generally, such a condition is forbidden for a particle that possess a charge under a $U(1)$ symmetry group, electromagnetism being one such group. However, for a particle that does not have such a charge, such a condition is entirely possible. If we consider a field whereby its left handed component and right handed components are not independent but rather $\psi_R = i\sigma^2{\psi^*}_L$, such a condition than becomes intrinsic. This is the Majorana condition and the spinor fields that follow it are known as Majorana fields that describe Majorana fermions or Majorana particles.

An interesting aspect of Majorana fermions is that they allow for mass terms with the same chiral state such as $m\overline{\psi_L}(\psi_L)^c = m\overline{\psi_L}\psi^c{}_R$. Another interesting aspect of Majorana fermions is that they violate lepton number symmetry which is a symmetry that states that the difference between the number of leptons and anti-leptons is conserved. This concludes the detour on Majorana fermions and we now move onto the actual focus of the chapter, which is on neutrino mass mechanisms.

Low Scale Type I Seesaw

We had considered the possibility of introducing a sterile right handed neutrino just to introduce a neutrino mass term above. Consider again, a right handed neutrino N_R, that forms Dirac mass terms with the regular neutrinos: $m_D\overline{\nu_L}N_R + h.c$. However, in such a model, there is nothing stopping a Majorana mass term involving just the newly introduced right handed neutrino N_R of the form $M\overline{(N_R)^c}N_R + h.c$.

To understand the mathematical formulation in a simplistic manner, we will consider a single ν and N, however the same formulation can be trivially extended to include 3 ν and an arbitrary number of N (whereby at least 2 are needed, as was explained in the last chapter). In this simplified formulation, the neutrino mass matrix can be given as: $[\bar{\nu} \quad \bar{N}]\begin{bmatrix} 0 & m_D \\ m_D & M \end{bmatrix}\begin{bmatrix} \nu \\ N \end{bmatrix}$. If we were to diagonalize the matrix $\begin{bmatrix} 0 & m_D \\ m_D & M \end{bmatrix}$, to the following form, $\begin{bmatrix} m_\nu & 0 \\ 0 & m_N \end{bmatrix}$, whereby we assume that $M \gg m_D$, we get $m_\nu \approx \frac{{m_D}^2}{M}$ and $m_N \approx M$. This is the crux of the simplest type of seesaw mechanism, where the largeness of M, the mass eigenvalue of heavy mass eigenstates, leads to the smallness of m_ν, the mass eigenvalue of the regular neutrinos. In literature, it is often found that the scale of $m_N \approx M$ be given as $\mathcal{O}(10^{14} - 10^{15})$.

This is based on the assumption that $y_{\nu N} \sim \mathcal{O}(1)$. Recall from last chapter that mass is proportional to the Yukawa coupling multiplied by the Higgs vacuum expectation value, which results in $m_D \sim y_{\nu N}.v$, where v is the vacuum expectation value of the Higgs field. Substituting the above approximate values and the vacuum expectation value of 246 GeV into $m_\nu \approx \frac{{m_D}^2}{M}$, gives the value of m_ν in the (sub) eV range, which is consistent with the upper bounds on neutrino masses. This is the well known high scale Type I seesaw mechanism. By introduction of at least two heavy mass eigenstates $N_i, i = 1, 2, \ldots$, it becomes possible to explain neutrino masses.

However, the choice of $y_{\nu N} \sim \mathcal{O}(1)$ is arbitrary. We could reasonably expect the Yukawa coupling of neutrinos to be the same order as that of electrons, i.e. $y_{\nu N} \sim y_e \sim \mathcal{O}(10^{-6})$, in which case the mass eigenvalue of the heavy neutrino mass eigenstate comes down to the ~ 10 - 100 GeV range. This constitutes the low scale Type I seesaw. A review of this model can be seen in [4]. Henceforth, within this thesis, the term Majorana heavy neutral lepton or Majorana HNL, will constitute referring to the heavy mass eigenstate of this class of neutrino mass models.

Inverse Seesaw

For describing this model, I will again stick to the use of a single generation of neutrinos to keep the notation simple and ensure the conceptual explanation is concise. In the inverse seesaw, instead of introducing one type of heavy mass eigenstate singlet N, a pair of heavy mass eigenstate singlets, N and S, are introduced. In this configuration, the lepton number of N can be given a value of 1 and the lepton number of S can be given a value of -1.

In this scenario, we could then write the neutrino mass matrix in the basis of $[\nu \quad N \quad S]$ as $\begin{bmatrix} 0 & m_D & 0 \\ m_D & \mu_N & m_R \\ 0 & m_R & \mu_S \end{bmatrix}$. Here m_D corresponds to the Dirac mass terms involving ν and N, m_R corresponds to Dirac mass terms of the form $m_R\left(\overline{(N_R)^c}S_R + \overline{(S_R)^c}N_R\right)$ and μ_N and μ_S correspond to Majorana mass terms for N and S. We consider the mass hierarchy of $\mu_N, \mu_S \ll m_D \ll m_R$. Furthermore, the contribution from μ_N to the masses of ν is minimal and for simplification, they can be taken as 0. With these assumptions and simplifications, the mass matrix can be diagonalized as $\begin{bmatrix} m_\nu & 0 & 0 \\ 0 & m_N & 0 \\ 0 & 0 & m_S \end{bmatrix}$ where $m_\nu \approx \mu_S \frac{{m_D}^2}{{m_D}^2+{m_R}^2}$ and $m_N, m_S \approx \sqrt{{m_D}^2 + {m_R}^2} \mp \frac{\mu_S}{2}\frac{{m_R}^2}{{m_D}^2+{m_R}^2}$. Here μ_S, the Majorana mass term, is sometimes also referred to as the lepton number violating parameter, and it is proportional to the mass eigenvalue of the light neutrinos. A review of this model can be found in [5].

It is the smallness of the Majorana mass term μ that leads to the smallness of the light neutrino masses, and therefore this model is referred to as the Inverse Seesaw model, in contrast to the Type I seesaw where the largeness of the Majorana mass term was responsible for smallness of the light neutrino mass terms. In the limit $\mu_S \to 0$, light neutrino mass eigenvalues become 0 and the heavy mass eigenstates N and S become degenerate. This is however, not what we want, as we went through all the effort just so that the light neutrino masses could be included in the theory in the first place.

However, for the theoretical calculations and experimental simulations and analysis part of this thesis, I will consider only a single heavy neutrino mass eigenstate. This simplifies the study, however it should be explicitly noted that since we are considering 'the heavy mass

term', we are in effect working in the $\mu_S \to 0$ limit, treating N and S as degenerate such that $m_N = m_S \approx \sqrt{{m_D}^2 + {m_R}^2}$. This is a small cost for the making this phenomenological study possible and accessible. From here on, the term Dirac heavy neutral lepton or Dirac HNL refers to the heavy mass eigenstate N or S, whereby the notation N will be consistently used henceforth.

Chapter 3: Theoretical Computations of the HNL

In the last chapter, we took a close look at the notion of a Dirac HNL and a Majorana HNL with a special focus on the mass terms of the specified neutrino eigenstates in question. In this chapter, the focus will shift onto the interaction terms.

The hypothesized heavy neutral leptons are sterile particles, and as a result do not directly interact with any Standard Model particles. Instead, their interactions happen through their mixing with the neutrino flavor eigenstates. In chapter 1, we took a brief look at the idea of how neutrinos mix between their flavor eigenstates and mass eigenstates and how this mixing is characterized by the terms of the mixing matrix U. Similarly, the mixing between the neutrino flavor eigenstates v_α and heavy neutrino mass eigenstates N_i where $\alpha = e, \mu, \tau$ and $i = 1, 2, 3 \ldots$ can be characterized with a mixing matrix V. In particular, the mixing expressions are given as:

$$|v_\alpha\rangle = \sum_i V_{\alpha i} \, |N_i\rangle$$

$$|N_i\rangle = \sum_\alpha V_{\alpha i}^* \, |v_\alpha\rangle$$

Combining this with the mixing between the flavor eigenstates and the light mass eigenstates, the following expression is obtained:

$$|v_\alpha\rangle = \sum_i U_{\alpha i} \, |v_i\rangle + \sum_j V_{\alpha j} \, |N_j\rangle$$

An interesting aspect about the Dirac and Majorana HNL interaction terms is that they are the same. This is because the interaction for both classes of HNLs is mediated through their

mixing with the flavor eigenstate. The differences we seek to find in the decays associated with Dirac vs Majorana HNLs will therefore not be due to differences in the interaction terms in the Lagrangian but rather be based on the allowed decay channels for the individual HNL. The Majorana HNL allows for lepton number violating decays whereas the Dirac HNL does not. The interaction Lagragian for the HNL (both Dirac and Majorana) including the various generations is given as:

$$\mathcal{L}_{N\,int} = -\frac{g}{\sqrt{2}} W_\mu{}^+ \sum_j \sum_{l=e,\mu,\tau} \bar{N}_j \, V_{lj}{}^* \gamma^\mu P_L l^- - \frac{g}{2\cos(\theta_w)} Z_\mu \sum_j \sum_{l=e,\mu,\tau} \bar{N}_j \, V_{lj}{}^* \gamma^\mu P_L v_l$$
$$- \frac{g m_N}{2\, m_W} h \sum_j \sum_{l=e,\mu,\tau} \bar{N}_j \, V_{lj}{}^* \gamma^\mu P_L v_l + h.c.$$

For the theoretical calculations and experimental simulations, I will focus on one generation of heavy neutral lepton, N_1 and its mixing with the electron neutrino. This approach is consistently followed throughout the thesis as explained in the previous chapter.

Feynman Rules

For interactions involving Dirac particles, the Feynman rules can be picked up directly from the Lagrangian. However, this is not the case for Majorana particles where it needs to be taken into account that they can undergo lepton number conserving or lepton number violating decays, and the rules for each of these channels is different. [6] provides a prescription for such interactions which will be discussed after looking at the explicit Feynman rules first.

From $\mathcal{L}_{N\,int}$, it is clear that the interaction terms involving N are exactly the same as the ones for the regular neutrino flavor eigenstates v, barring the V^*. In particular, where the fermion

flow arrow of the HNL is directed away from the vertex, the term V^* comes into effect, and where the fermion flow arrow is pointed towards the vertex, its conjugate V comes into effect. To summarize, the following are the Feynman rules for vertices:

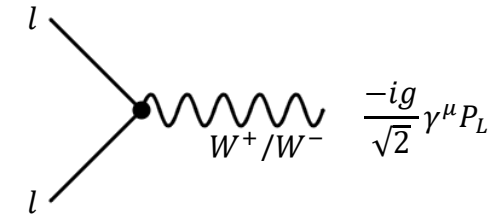

$$\frac{-ig}{\sqrt{2}}\gamma^\mu P_L$$

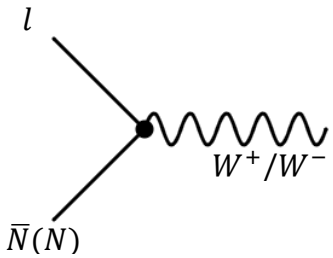

$$\frac{-ig}{\sqrt{2}}V^*(V)\gamma^\mu P_L$$

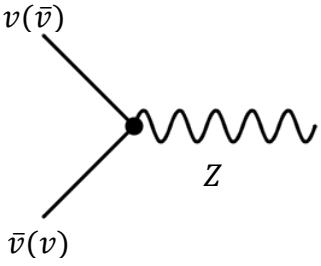

$$\frac{-ig}{2\cos(\theta_w)}\gamma^\mu P_L$$

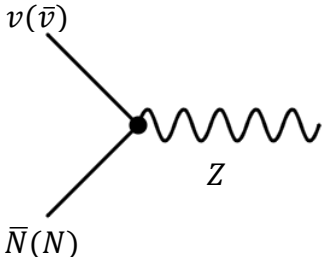

$$\frac{-ig}{\cos(\theta_w)}V^*(V)\gamma^\mu P_L$$

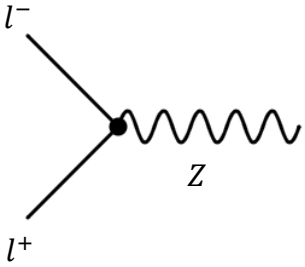

$$\frac{-ig}{2\cos(\theta_w)}\gamma^\mu\left(2\,sin^2(\theta_w)-\frac{1}{2}+\frac{1}{2}\gamma^5\right)$$

The rule for the force mediating massive vector bosons is as follows:

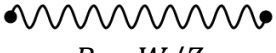

$$\frac{-ig_{\mu\nu}+q_\mu q_\nu/{M_{boson}}^2}{q^2-{M_{boson}}^2}$$

A point to note is that the diagrams involving Higgs boson are not being considered as they will have very negligible effect due to the Yukawa coupling of electron being very small.

The rules for the external spinors are usually given as $\bar{u}/u$ for particles and $v/\bar{v}$ for antiparticles, however, the computation in this chapter will be performed explicitly in helicity basis and hence the rules for the spinors with explicit left or right handedness need to be looked at as follows:

For incoming particles:

$$u_L = \begin{bmatrix} -\sqrt{E+m}\sin\left(\frac{\theta}{2}\right) \\ \sqrt{E+m}\,e^{i\phi}\cos\left(\frac{\theta}{2}\right) \\ \frac{P}{\sqrt{E+m}}\sin\left(\frac{\theta}{2}\right) \\ -\frac{P}{\sqrt{E+m}}e^{i\phi}\cos\left(\frac{\theta}{2}\right) \end{bmatrix}; \qquad u_R = \begin{bmatrix} \sqrt{E+m}\cos\left(\frac{\theta}{2}\right) \\ \sqrt{E+m}\,e^{i\phi}\sin\left(\frac{\theta}{2}\right) \\ \frac{P}{\sqrt{E+m}}\cos\left(\frac{\theta}{2}\right) \\ \frac{P}{\sqrt{E+m}}e^{i\phi}\sin\left(\frac{\theta}{2}\right) \end{bmatrix}$$

For outgoing particles:

$$\overline{u_L} = \begin{bmatrix} -\sqrt{E+m}\sin\left(\frac{\theta}{2}\right) & \sqrt{E+m}\,e^{-i\phi}\cos\left(\frac{\theta}{2}\right) & -\frac{P}{\sqrt{E+m}}\sin\left(\frac{\theta}{2}\right) & \frac{P}{\sqrt{E+m}}e^{-i\phi}\cos\left(\frac{\theta}{2}\right) \end{bmatrix};$$

$$\overline{u_R} = \begin{bmatrix} \sqrt{E+m}\cos\left(\frac{\theta}{2}\right) & \sqrt{E+m}\,e^{-i\phi}\sin\left(\frac{\theta}{2}\right) & -\frac{P}{\sqrt{E+m}}\cos\left(\frac{\theta}{2}\right) & -\frac{P}{\sqrt{E+m}}e^{-i\phi}\sin\left(\frac{\theta}{2}\right) \end{bmatrix}$$

For outgoing antiparticles (i.e. inward pointing antiparticles):

$$v_L = \begin{bmatrix} \frac{P}{\sqrt{E+m}}\cos\left(\frac{\theta}{2}\right) \\ \frac{P}{\sqrt{E+m}}e^{i\phi}\sin\left(\frac{\theta}{2}\right) \\ \sqrt{E+m}\cos\left(\frac{\theta}{2}\right) \\ \sqrt{E+m}\,e^{i\phi}\sin\left(\frac{\theta}{2}\right) \end{bmatrix}; \qquad v_R = \begin{bmatrix} \frac{P}{\sqrt{E+m}}\sin\left(\frac{\theta}{2}\right) \\ -\frac{P}{\sqrt{E+m}}e^{i\phi}\cos\left(\frac{\theta}{2}\right) \\ -\sqrt{E+m}\sin\left(\frac{\theta}{2}\right) \\ \sqrt{E+m}\,e^{i\phi}\cos\left(\frac{\theta}{2}\right) \end{bmatrix}$$

For incoming antiparticles (i.e. outward pointing antiparticles):

$$\overline{v_L} = \left[\frac{P}{\sqrt{E+m}}\cos\left(\frac{\theta}{2}\right) \quad \frac{P}{\sqrt{E+m}}e^{-i\phi}\sin\left(\frac{\theta}{2}\right) \quad -\sqrt{E+m}\cos\left(\frac{\theta}{2}\right) \quad -\sqrt{E+m}\,e^{-i\phi}\sin\left(\frac{\theta}{2}\right)\right];$$

$$\overline{v_R} = \left[\frac{P}{\sqrt{E+m}}\sin\left(\frac{\theta}{2}\right) \quad -\frac{P}{\sqrt{E+m}}e^{-i\phi}\cos\left(\frac{\theta}{2}\right) \quad \sqrt{E+m}\sin\left(\frac{\theta}{2}\right) \quad -\sqrt{E+m}\,e^{-i\phi}\cos\left(\frac{\theta}{2}\right)\right]$$

All the above rules have been given without any derivations as they can easily be found in many standard Quantum Field Theory or Particle Physics textbooks. These rules apply directly to interactions involving Dirac particles. For interactions involving Majorana particles, [6] provides a prescription that can be used for interactions involving Majorana particles. In particular, the effect of the prescription is as follows:

- For each diagram, define a fermion flow (given as red lines in the diagrams that follow). This is trivial for a lepton number conserving interaction, whereby just the arrows on the Feynman diagram can be followed, however, for lepton number violating diagrams, the direction of the flow can be chosen arbitrarily (which then has an impact on which spinors to choose). For the computations in this project, I stick to using the fermion flow that is consistent with the corresponding lepton number conserving diagram. (This will become clearer in the next few sections.)
- Based on the above convention, for lepton number conserving diagrams, fermion flow will match the arrows in the diagram and the vertex terms will be used as they are. However, for lepton number violating, the fermion flow will oppose the arrows in the diagram and vertex terms will need to be modified. The modification as proposed in [6] has a simple effect in the computations of interest to us: P_L is changed to $-P_R$ in the vertex terms.

- For the spinors of lepton number conserving diagrams, spinors will be used conventionally, however, for lepton number violating decays, as our defined fermion flow is in the opposite direction of the arrows in the diagram, we treat the (incoming)outgoing particles as (incoming)outgoing antiparticles and vice versa. A simple justification for this prescription is given in [7].

With this we are now ready to take a look at the Feynman diagrams of interest.

Feynman Diagrams

The number of diagrams involved in the computation are 12 for the Majorana HNL and 6 for the Dirac HNL. The following method is used for labelling them:

- Odd numbered diagrams correspond to lepton number conserving diagrams and even numbered diagrams correspond to their lepton number violating counterparts
- Diagrams 1-4 involve neutral current decays, hence they are divided into left handed and right handed diagrams corresponding to the handedness of the final state electron and positron
- Diagram 5-8 involve charged current decays and as such they only allow final state left handed particles and right handed antiparticles

The diagrams as are follows:

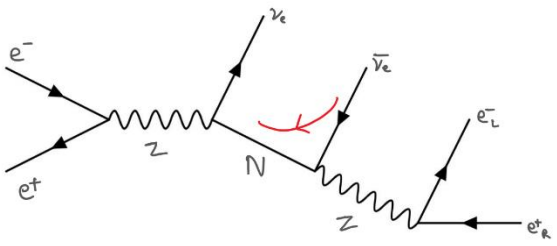

Fig. 3.1: Diagram 1L

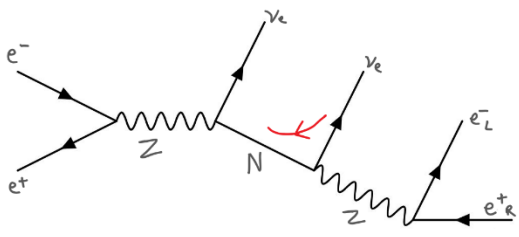

Fig. 3.2: Diagram 2L

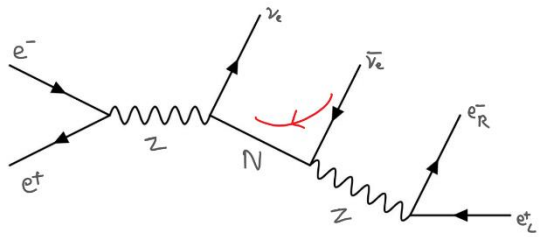

Fig. 3.3: Diagram 1R

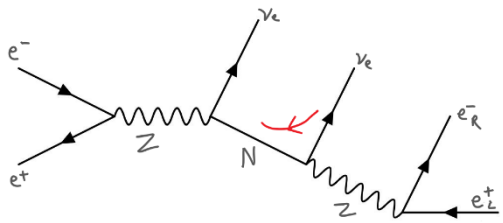

Fig. 3.4: Diagram 2R

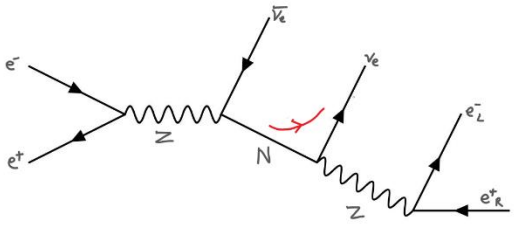

Fig. 3.5: Diagram 3L

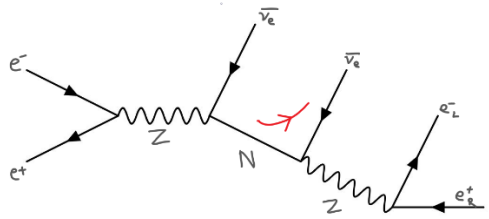

Fig. 3.6: Diagram 4L

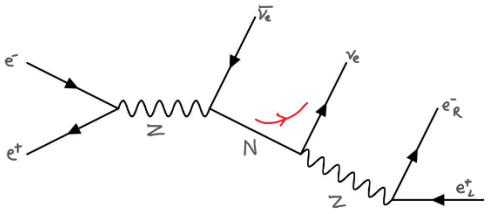

Fig. 3.7: Diagram 3R

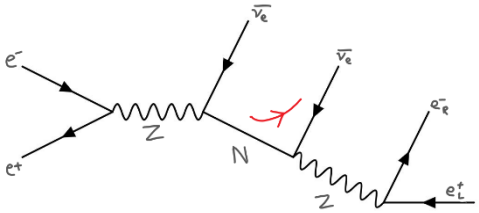

Fig. 3.8: Diagram 4R

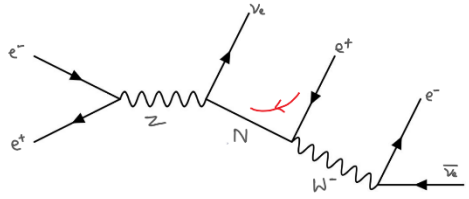

Fig. 3.9: Diagram 5

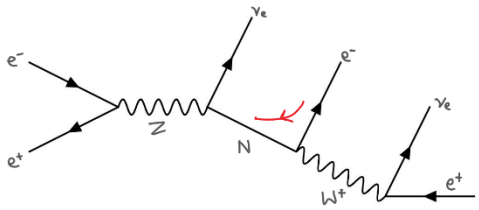

Fig. 3.10: Diagram 6

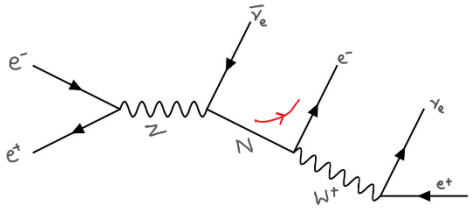

Fig. 3.11: Diagram 7

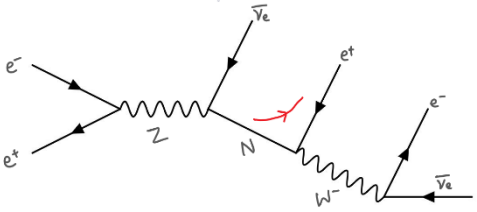

Fig. 3.12: Diagram 8

Amplitudes

The HNLs in the above diagrams are on shell long lived particles, and as a result, to study the difference between Dirac vs Majorana HNLs, it suffices to compute the amplitude corresponding to the three body decay of the HNL, and the production of the HNL does not need to be included. Computation of all the amplitudes (and decay widths) are shown in Appendix A, however for the purposes of understanding, I will briefly demonstrate the process of computing the amplitudes for Diagram 1L and Diagram 2L as a means to show how lepton number violating channels are treated according to the prescription which was described in the Feynman rules section above.

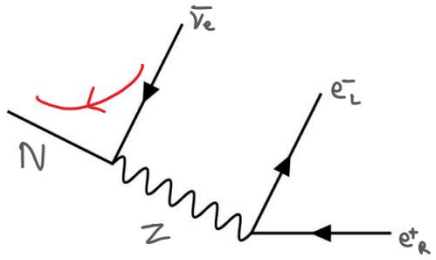

Fig. 3.13: Diagram 1L- HNL decay

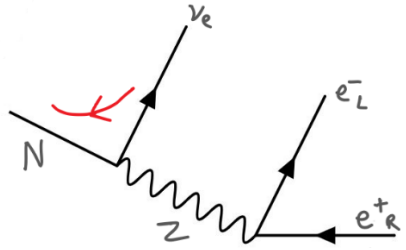

Fig. 3.14: Diagram 2L- HNL decay

The fermion lines in the above diagram become specially important now because they are the only way of identifying whether the decay corresponds to a lepton number conserving or lepton number violating channel.

Based on the Feynman rules and the prescription, given above, for treating lepton number violating processes, the amplitudes are as follows:

$$\mathcal{M}_{1L} = \overline{\nu_R}(p_N) * \frac{-ig}{2\cos(\theta_w)} V^* \gamma^\mu P_L * \nu_R(p_{\bar{\nu}}) * \frac{-ig_{\mu\nu}}{q^2 - {M_Z}^2} * \overline{u_L}(p_{e^-}) * \frac{-ig}{2\cos(\theta_w)} \gamma^\mu \left(2\sin^2(\theta_w) - \frac{1}{2} + \frac{1}{2}\gamma^5\right) * \nu_R(p_{e^+})$$

$$\mathcal{M}_{2L} = \overline{v_L}(p_N) * \frac{-ig}{2\cos(\theta_w)} V^* \gamma^\mu (-P_R) * v_L(p_v) * \frac{-ig_{\mu\nu}}{q^2 - {M_Z}^2} * \overline{u_L}(p_{e^-}) * \frac{-ig}{2\cos(\theta_w)} \gamma^\mu \left(2\,sin^2(\theta_w) - \frac{1}{2} + \frac{1}{2}\gamma^5\right) * v_R(p_{e^+})$$

The highlighted terms above correspond to the prescription described above on how lepton number violating processes are treated. After following this process for all the diagrams, amplitudes have to be squared with appropriate diagrams that interfere clubbed together. In particular, for the Majorana HNL:

$${\mathcal{M}_{N\,maj}}^2 = (\mathcal{M}_{1L} + \mathcal{M}_5)^2 + (\mathcal{M}_{2L} + \mathcal{M}_6)^2 + (\mathcal{M}_{3L} + \mathcal{M}_7)^2 + (\mathcal{M}_{4L} + \mathcal{M}_8)^2 + {\mathcal{M}_{1R}}^2 + {\mathcal{M}_{2R}}^2 + {\mathcal{M}_{3R}}^2 + {\mathcal{M}_{4R}}^2$$

For the Dirac HNL:

$${\mathcal{M}_{N\,dir}}^2 = (\mathcal{M}_{1L} + \mathcal{M}_5)^2 + (\mathcal{M}_{3L} + \mathcal{M}_7)^2 + {\mathcal{M}_{1R}}^2 + {\mathcal{M}_{3R}}^2$$

With the squared amplitudes computed, we proceed with the phase space integration and computation of differential decay width.

Phase space and differential decay width

To obtain the decay width or the differential decay width of a particle, its squared amplitude has to be integrated over the phase space. The squared amplitude above consists of 9 phase space variables ($p_e,\ p_p,\ p_v,\ \theta_e,\ \theta_p,\ \theta_v,\ \phi_e,\ \phi_p,\ \phi_v$) and 1 fixed variable m_N. Note that we work in the rest frame of the HNL and the final state particles are treated as massless. However, these 9 variables are not independent degrees of freedom. A 3 body decay has a phase space characterized by 5 independent variables. Before looking at these variables, a subtle yet important note: (anti)neutrinos are invisible in collider experiments and as such

their kinematical variables can not be obtained, hence in the amplitude and differential decay width calculations, no distinctions are made between momentum, polar angle and azimuthal angle for neutrinos and anti neutrinos. Their properties are correctly captured by the appropriate usage of particle or anti particle spinors and it is completely fine to label their four momentum components as just v, thereby having a final amplitude and differential decay width that does not discriminate between neutrinos and anti neutrinos.

The 1 fixed variable, is, as its name suggests, fixed by the mass of the HNL. The 5 phase space variables can however be chosen based on the purposes of the study. An example of differential decay width with respect to 5 phase space variables as shown in [8] is as follows:

$$\partial\Gamma = \frac{1}{(2\pi)^5}\frac{1}{16M}|M|^2\,\partial E_1\,\partial E_2\,\partial\alpha\,\partial\cos(\beta)\,\partial\gamma$$

Here the decay phase space is parametrized by the energies of the 2 out of the 3 final state particles, and by the 3 Euler angles (note that a 3 body decay lies on a plane and the orientation of any plane can be characterized by 3 Euler angles).

Here it becomes useful to consider the specific phase space variables to choose. The difference between Majorana and Dirac HNLs is that of lepton number conserving + lepton number violating decays vs just lepton number conserving decays respectively. The 'lepton number violating' processes become possible by the condition $\psi^c = \psi$, which was explained in the previous chapter. To make physical sense out of this mathematical condition, the Majorana condition can be interpreted as the possibility of a Majorana particle to undergo a spin (and hence helicity) flip as it propagates. Since the Dirac vs Majorana difference is linked to the spin, it is a good choice to opt for phase space variables linked to angular distributions.

Consider a triangle which has a fixed parameter. The lengths of its sides are intimately linked with the angles between its sides. We can use this observation for the 3 body decay on a plane because, when the momentum vectors of the 3 final state particles are placed tail to head, it has to form a closed triangle (due to conservation of momentum and decaying particle being at rest) and the sum of the lengths of the sides of the triangle has to be fixed (conservation of energy whereby the momentum of final state particles is derived from the mass of the HNL). As a result, we can parametrize the 3 body decay on a plane by angles between 2 pairs of particles, for instance θ_{ee} and θ_{ev} where θ_{ee} is the angle between the electron and the positron, and θ_{ev} is the angle between the electron and the (anti)neutrino. Technically, θ_{ee} and θ_{ev} are also not completely independent, as the integration over one of the variables has limits involving the other variable.

We now have 5 phase space variables $\theta_{ee}, \theta_{ev}, \alpha, \beta$ and γ. There is however, a rotational invariance about the spin axis of the decaying particle, which allows reducing the phase space to just 4 variables. This can be achieved by setting the azimuthal angle of one of the particles to 0. Before that, all these angles need to be linked to the 9 variables in the amplitude. First step would be to link $\alpha = \phi_e = 0$, where it is set to 0 using the rotational invariance of the system. Second, we can choose $\beta = \theta_e$. Next, we define the system on the y-z plane where the p_e lies on the positive z-axis. Without loss of generality, we can define the positive y direction to be the direction where the positron's momentum vector lies and the negative y direction to be where the (anti)neutrino's momentum vector lies. Then we rotate the y-z plane about the z-axis by γ followed by a rotation about the y-axis by θ_e. This explanation has qualitatively provided the link between 9 variables from the amplitude calculation to the 5 phase space variables of our choice as follows:

1. $p_e = \frac{-m_N \sin(\theta_{ee}+\theta_{ev})}{\sin(\theta_{ev}) + \sin(\theta_{ee}) - \sin(\theta_{ee}+\theta_{ev})}$
2. θ_e as is
3. $\phi_e = 0$
4. $p_p = \frac{m_N \sin(\theta_{ev})}{\sin(\theta_{ev}) + \sin(\theta_{ee}) - \sin(\theta_{ee}+\theta_{ev})}$
5. $\theta_p = arc\cos\big(sin(\theta_e)\, sin(\gamma) sin(\theta_{ee}) + cos(\theta_e) cos(\theta_{ee})\big)$
6. $\phi_p = arc\sin\left(\frac{cos(\gamma)\, sin(\theta_{ee})}{sin(\theta_p)}\right)$
7. $p_v = m_N - p_e - p_p$
8. $\theta_v = arc\cos(cos(\theta_e)\, cos(\theta_{ev}) - sin(\theta_e)\, sin(\gamma)\, sin(\theta_{ev}))$
9. $\phi_v = arc\sin\left(\frac{-cos(\gamma)\, sin(\theta_{ev})}{sin(\theta_v)}\right)$

With this, all variables have now been defined in terms of the phase space variables and the phase space integration can be performed to obtain Γ or $\frac{\partial \Gamma}{\partial \theta_{ee}}$. The formula that was provided above for the differential decay width can be used for the integration, however, the change of variables needs to be accounted for by multiplication with the determinant of the Jacobian matrix. The entire calculation is provided in Appendix A.

Results

Since the results are directly based on the calculations done in Appendix A, I would like to clarify a few points before presenting the results.

- In the full calculation, θ_e and ϕ_e were directly taken as Euler angles without the use of α or β. The angle referred to as γ above is denoted as β in the calculations in Appendix A.

- It was seen that amplitudes have a V or a V^* factor. When the amplitudes are squared, the amplitude expression in multiplied by its complex conjugate and therefore every squared amplitude term contains V^*V as a multiplicative factor. This value of mixing angle gives a model dependence to the results as it directly affects the decay width and the differential decay. The entire calculation can be performed without any reference to V or V^* and at the end V^*V can be multiplied to Γ or $\frac{\partial \Gamma}{\partial \theta_{ee}}$. However, the results present are of normalized differential decay width i.e. $\frac{1}{\Gamma}\frac{\partial \Gamma}{\partial \theta_{ee}}$. This characterizes the difference between Dirac HNL decays and Majorana HNL decays without the model dependent V^*V term and as a result, in the calculations in Appendix A, V or V^* are not present.
- The choice of normalized differential decay width is necessary as the decay width (and therefore the differential decay width) of the Dirac and Majorana HNL differ by a factor of ~2. This is due to that fact that Majorana HNL has twice the decays modes as that of the Dirac HNL.

The normalized differential decay widths for 20, 50 and 70 GeV HNLs are as below:

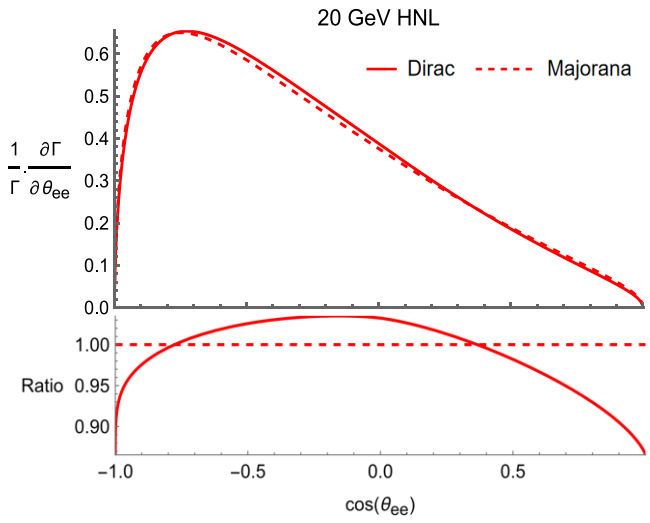

Fig. 3.15: Differential decay width (20 GeV)

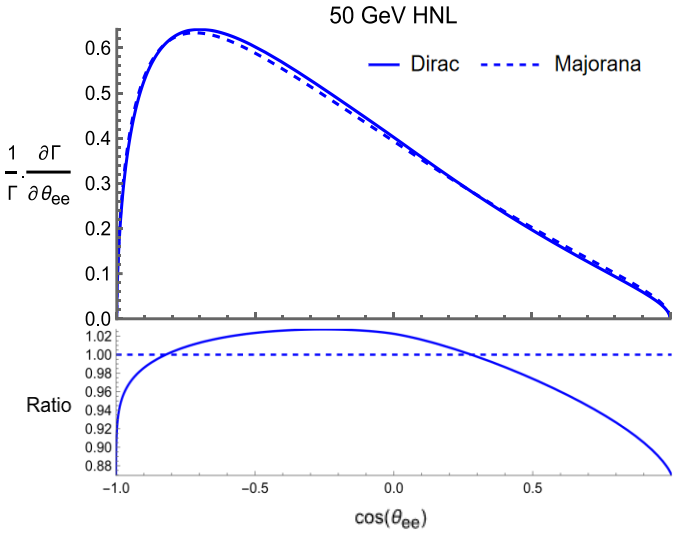

Fig. 3.16: Differential decay width (50 GeV)

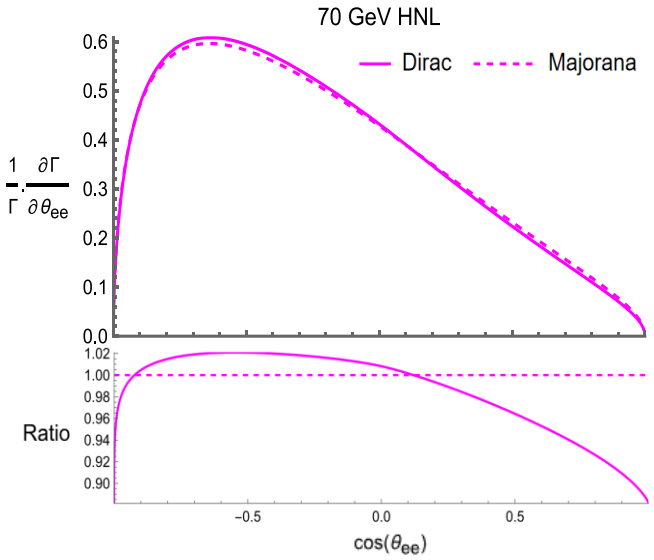

Fig. 3.17: Differential decay width (70 GeV)

All the three plots show differences between the Dirac and Majorana HNL, however, these plots can not be directly compared with experimental or simulated data. Real experimental data or Monte Carlo simulated data would involve an HNL that has a large momentum which would modify the angular distributions(boost modifies angular distances). Furthermore, considering the HNL production happens at a specific energy, the largeness of the momentum of the HNL would depend on the smallness of the mass of the HNL, and as a result, HNLs corresponding to different masses would be boosted by different amounts

leading to different levels of modification to the angular distribution plots. As such, we proceed by interpreting the results obtained in the above computations and use the interpreted conclusions for comparison with experimental studies.

The observations and interpretations are as follows:

- The differential decay width for all masses shows a higher value for the Dirac HNL at larger angles and conversely shows a higher value for the Majorana HNL at smaller angles (barring the range of -1 to -0.8 for $\cos(\theta_{ee})$). In experimental or simulated data, a higher differential decay width would translate to a higher number of events.
- The angle at which the differential decay widths of Dirac and Majorana HNLs cross (the second time) appears to increase slightly as the mass of the HNL increases.
- The differential decay widths do indeed differ, but the differences appear to be very little. It is imperative to study this variable in Monte Carlo generated events to see whether the difference is enough to have a decent discriminating potential.

With this, the theoretical section of this thesis concludes and in the next chapter, the focus will shift to the experimental aspects of the project.

Chapter 4: Introduction to FCC-ee and the FCC Framework

The Future Circular Collider is a planned collider by CERN that will succeed the Large Hadron Collider. The Large Hadron Collider has been of immense importance to particle physics, most specifically due to its discovery of the Higgs Boson, which completed the Standard Model of Particle Physics. However, as of the writing of this thesis, there has not been a single discovery of any Beyond the Standard Model particles. Due to many open problems that can not be explained by the Standard Model, it becomes imperative to study BSM models that could indeed explain physical observations. The lack of discovery of any BSM particles hints at two possibilities for the nature of such particles that is, either they are heavier than the existing energy reach or they are very weakly coupled to SM particles. Without any reason to pick one possibility over the other, it becomes necessary to look at a collider that can access higher energies and higher luminosities and this is why the planned FCC is going to be a very important laboratory.

It is useful to picture the FCC in comparison to the LHC. The LHC was preceded by the Large Electron Positron Collider (LEP). Previously LEP and now the LHC run in the same 27 km tunnel. The center of mass energy of LEP was 209 GeV whereas for the LHC, it is 13-14 TeV. Similarly, the FCC is planned to be run as an electron positron collider, the FCC-ee, followed by a hadronic collider, the FCC-hh. The energy range of FCC-ee is planned to be from 90 to 350 GeV whereby it will run at different center of mass energies at different periods of time. The planned center of mass energy of FCC-hh is 100 TeV. As evident from these values, the FCC project would therefore tremendously increase the reach of physics in terms of energy scales and cross sections.

The study within this thesis has focused on the searches for HNL at the FCC-ee and therefore, I would like to go over some aspects of the FCC-ee in details, that explain why it provides an optimum environment for searches of HNL within the 10s of GeV mass scale.

Aspects of FCC-ee

The FCC-ee is proposed to be a high luminosity, and wide energy range electron positron collider that focuses on studying the Z boson, W boson, Higgs boson and top quark. It is estimated that it would produce on the order of: ~ 5e12 Z bosons, 1e8 W bosons, and 1e6 Higgs bosons and top quarks each. This is implemented in several stages by running the collider at specific energy scales including the Z pole (91 GeV), WW threshold (161 GeV), HZ production peak (240 GeV) and $t\bar{t}$ threshold (350 GeV) and above. At the Z pole and WW threshold, the machine would run at the center of mass energy calibrated to the precision of the order of 100 keV. The aim of these runs is precision measurements and new physics searches. New physics searches offer a direct glance at new particles whereas precision measurements allow for constraining of known physical parameters and also for detecting deviations from theoretical predictions, which is a good signature for new physics.

In the context of the searches pertaining to heavy neutral leptons/heavy neutrinos/right handed neutrinos/sterile neutrinos, based on our current experimental data, these particles would be quite difficult to produce, however the energy reach, the very high luminosity and the very nature of leptonic collider providing a relatively clean background environment makes the FCC-ee a perfect avenue for such explorations. The very nature of weakly coupled sterile neutrinos is related to their small mixing angles and this translates to them being long lived particles and consequently leading to displaced vertex searches which makes the

detection environment even clearer. Based on the planned luminosity of 150 ab^{-1} [9] of the Tera-Z run at the FCC-ee, we obtain the following number of HNLs produced for different mixing angles at the HNL mass of 50 GeV [17] without any event selection:

Mixing Angle V_eN	Cross section (pb)	No. of events
1.00E-01	2.29	343200000
1.00E-02	2.29E-02	3432000
1.00E-03	2.29E-04	34320
1.00E-04	2.29E-06	343
1.00E-05	2.29E-08	3
1.00E-06	2.29E-10	0

Table 4.1: Cross section and expected number of events for particular values of mixing angles V_eN

It becomes evident from these numbers that the FCC-ee provides for a great environment to search for heavy neutral leptons.

Simulation and Analysis

The process of simulation begins by using Madgraph [10, 11] and Pythia [12] to generate a Les Houches Event file that contains kinematical variables of particles involved in the process of collisions and decays. To generate the processes involving a Majorana HNL, the HeavyN [13, 14] Universal FeynRules Object model is used, and to generate Dirac HNL, the HeavyN Dirac [5] Universal FeynRules Object model is used. The .lhe file format is then passed on to Delphes [15] for the detector simulation, whereby the IDEA detector [16] card is used for the response simulation. The final output is an EDM4HEP format file. The final analysis is conducted using the FCC framework that uses the EDM4HEP format and is able to generate all the variables of interest by the use of a Python Script, that is customized as per the analysis needs.

The Process

We base our analysis on the purely leptonic decay channel of the HNL. This choice is motivated by the structure of the FCC Framework at the time the analysis was conducted. In order to retrieve a process, a function of 'exclusive decay' was used which required the user to specify the exact particles produced in the process. This is a simple task for a leptonic decay channels but becomes extremely complex for semi leptonic or purely hadronic channels given the wide range of ways in which quarks could be produced. This however leaves a possible avenue for future study upon the inclusion of an 'inclusive decay' function within the FCC Analysis framework which could be used to conduct a study on the hadronic decay modes.

The analysis in this study focuses on the 2 to 4 body decay processes involving the HNL as specified below.

The process for the Majorana HNL is:

$e^- e^+ \rightarrow Z \rightarrow N\,\nu + N\,\overline{\nu}$ where $N \rightarrow e^- e^+ \nu + e^- e^+ \overline{\nu}$

The process for the Dirac HNL is:

$e^- e^+ \rightarrow Z \rightarrow \overline{N}\,\nu + N\,\overline{\nu}$ where $N(\overline{N}) \rightarrow e^- e^+ \nu(\overline{\nu})$

This is due to the previously stated fact about the nature of these particles, i.e. the Majorana HNL undergoes lepton number conserving and lepton number violating decay processes whereas the Dirac HNL undergoes only lepton number conserving decay processes.

Analysis specifics

It is important to note that in collider experiments, neutrinos and anti neutrinos are invisible as they pass through the different layers of the detector without interacting. This means that the lepton number conservation or violation can not be deduced and by extension the Majorana or Dirac nature of the decaying particle can not be deduced by observing the lepton number conservation or violation. This results in the analysis being restricted to only the charged leptons produced in the decay of the HNL. After the generation of the sample files following the procedure as stated in the above section, the sample files are used to extract event wise global variables and kinematical variables pertaining to the charged leptons, i.e. electrons and positrons. In particular, we are able to obtain variables including (but not limited to) the lifetime of the HNL, transverse distance traversed by the HNL before decaying, missing transverse energy, individual components of the four momentum of the daughter particles, etc. This lays the groundwork for the next chapter where we discuss in details the specific results obtained from the above specified analysis.

Chapter 5: HNL Simulations and Analysis

The focus of this chapter are the results obtained from the experimental simulation and analysis (as explained in last chapter). The analysis is performed on Dirac and Majorana HNLs with masses of 20 GeV, 50 GeV and 70 GeV considering only the leptonic decay channel:

$$e^- e^+ \rightarrow Z \rightarrow N\, \nu/\overline{\nu} \rightarrow e^- e^+ \nu/\overline{\nu}\, \nu/\overline{\nu}$$

It is worth considering whether the same decay process provides equivalent information across the mass ranges of 20-70 GeV. To answer this question, the branching ratios of HNL with masses ranging from 10 GeV to the W boson mass were considered for the following channels:

- $N \rightarrow q\, q\, l$
- $N \rightarrow q\, q\, \nu$
- $N \rightarrow l\, l\, \nu$
- $N \rightarrow \nu\, \nu\, \nu$

Where q, l and ν take into account particles and anti-particles of all generations. The branching ratios were obtained using Madgraph [10, 11] with the HeavyN [13, 14] Universal FeynRules Object model. The results obtained are shown in Fig. 5.1. This figure shows that the branching ratios for HNLs are more or less the same and therefore the analysis of 20, 50 and 70 GeV can be looked at together. The branching ratios are independent of the mixing angles of the HNLs.

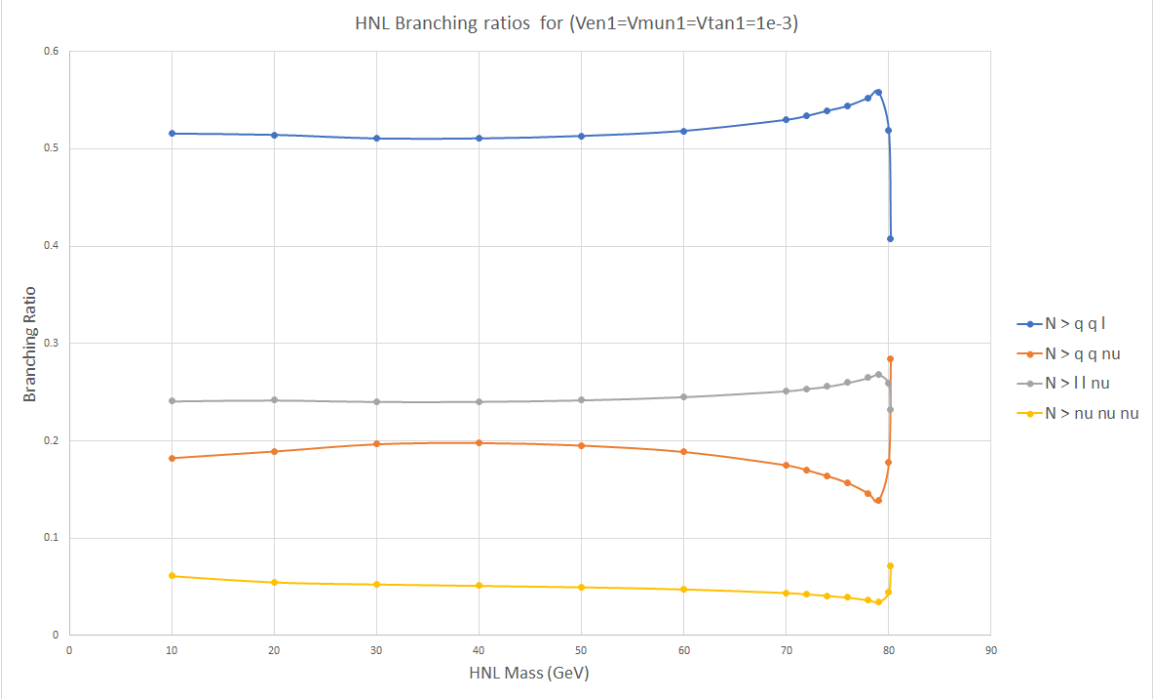

Fig. 5.1: HNL Branching ratios as a function of mass

The analysis begins by looking at the distributions of the final state leptons' variables, namely $p_x, p_y, p_z, pT, \theta, \varphi$ and E of the reconstructed final state electrons and positrons. It would be natural to expect the φ distributions to not show any differences as the decay processes for both, Majorana and Dirac HNLs, would have a rotational symmetry about the beam axis. This can be seen for electrons and positrons in Fig. 5.2a and 5.2b for 20 GeV, Fig. 5.3a and 5.3b for 50 GeV and Fig. 5.4a and 5.4b for 70 GeV cases respectively.

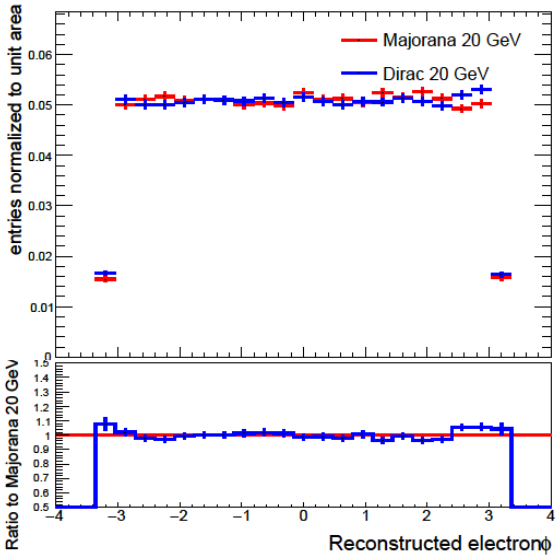

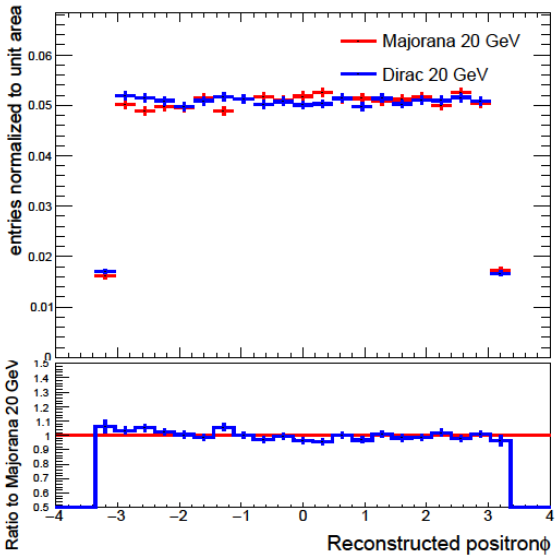

Fig. 5.2a (left): φ distribution of final state electrons, Fig. 5.2b (right): φ distribution of final state positrons

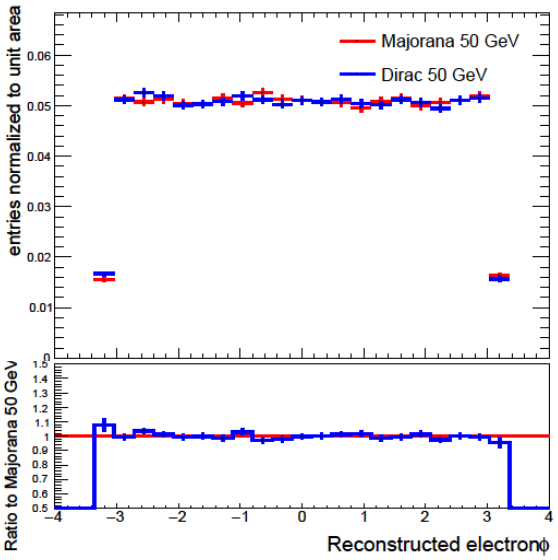

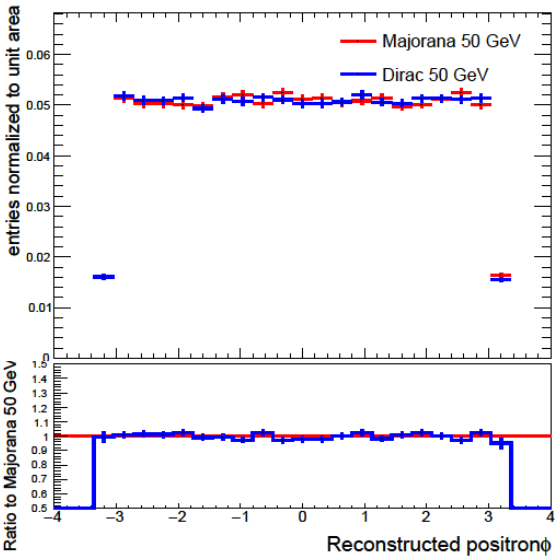

Fig. 5.3a (left): φ distribution of final state electrons, Fig. 5.3b(right): φ distribution of final state positrons

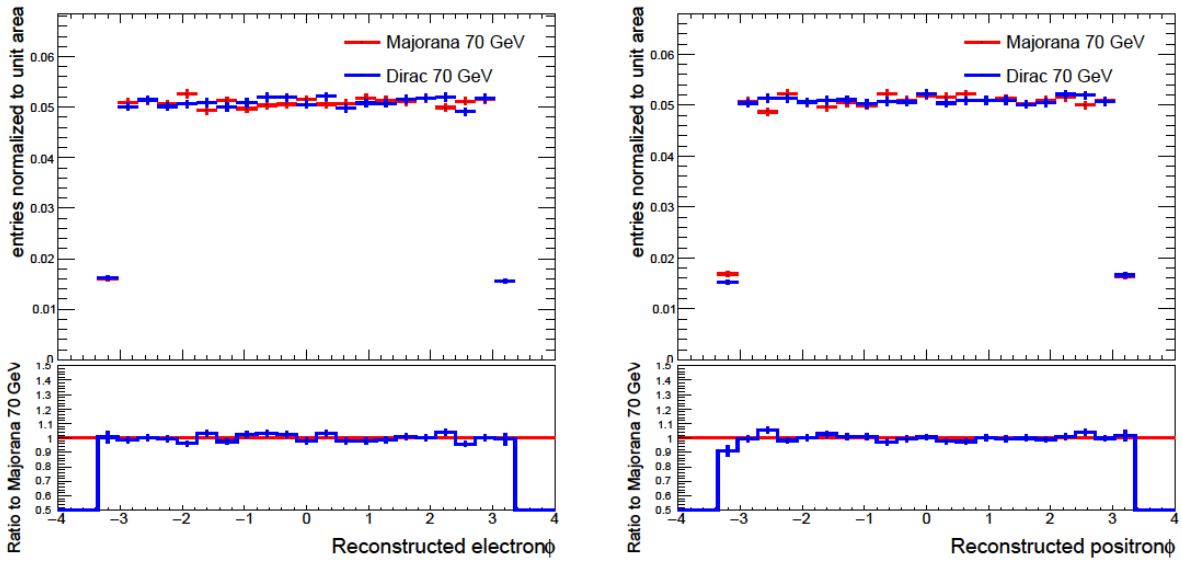

Fig. 5.4a (left): φ distribution of final state electrons, Fig. 5.4b(right): φ distribution of final state positrons

All the other final state leptons' variables will now be looked at, and based on theoretical studies, that predict a difference in angular distribution variables, it could be expected that all these variables should show differences between Majorana and Dirac cases.

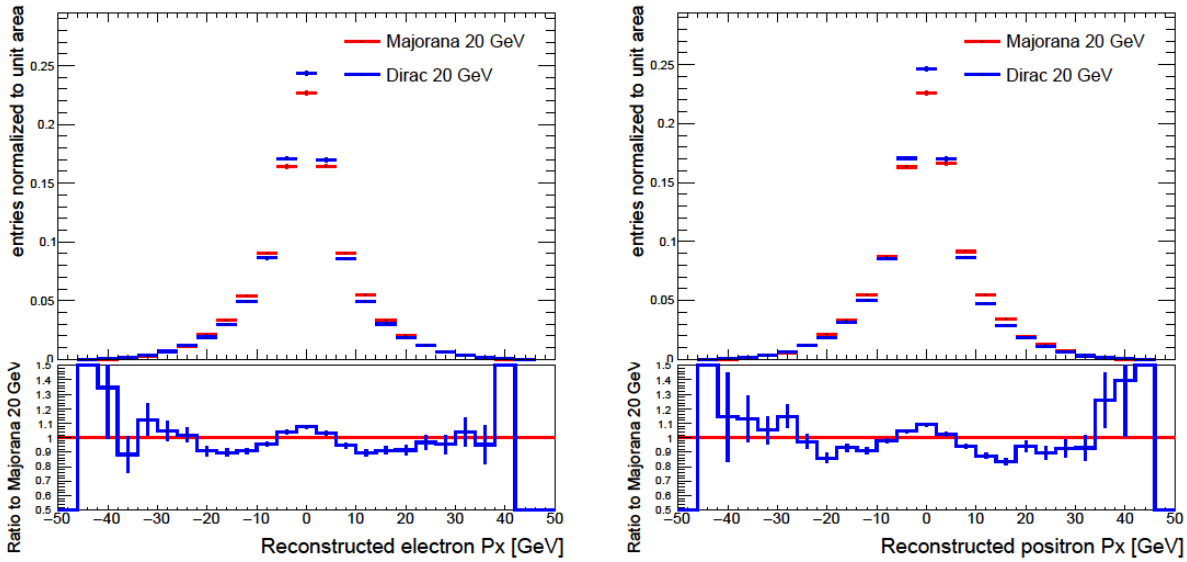

Fig. 5.5a (left): p_x distribution of final state electrons, Fig. 5.5b(right): p_x distribution of final state positrons

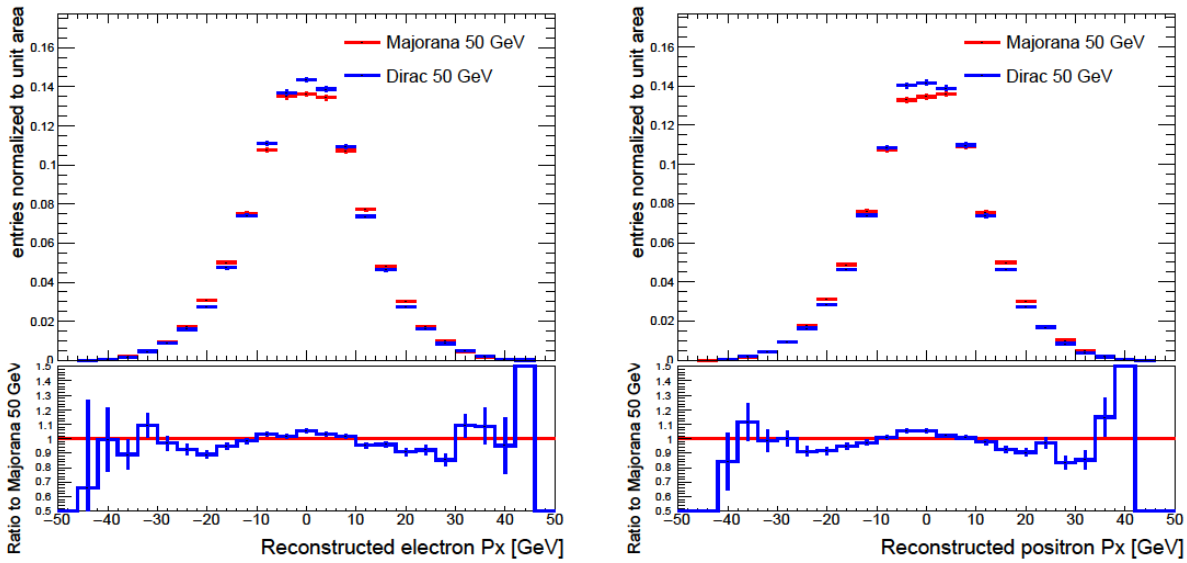

Fig. 5.6a (left): p_x distribution of final state electrons, Fig. 5.6b(right): p_x distribution of final state positrons

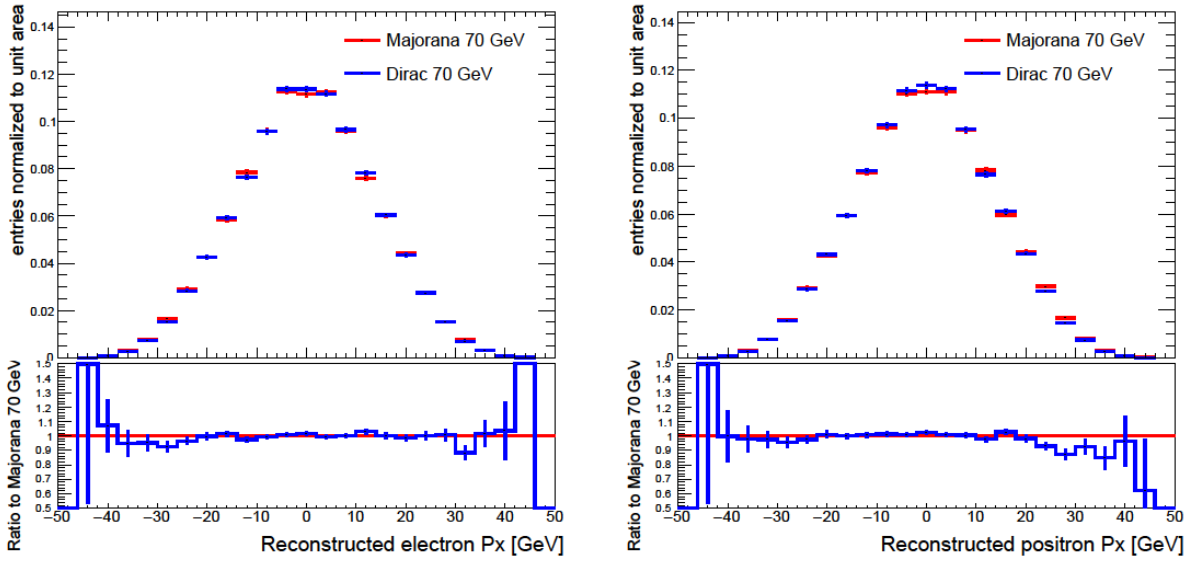

Fig. 5.7a (left): p_x distribution of final state electrons, Fig. 5.7b(right): p_x distribution of final state positrons

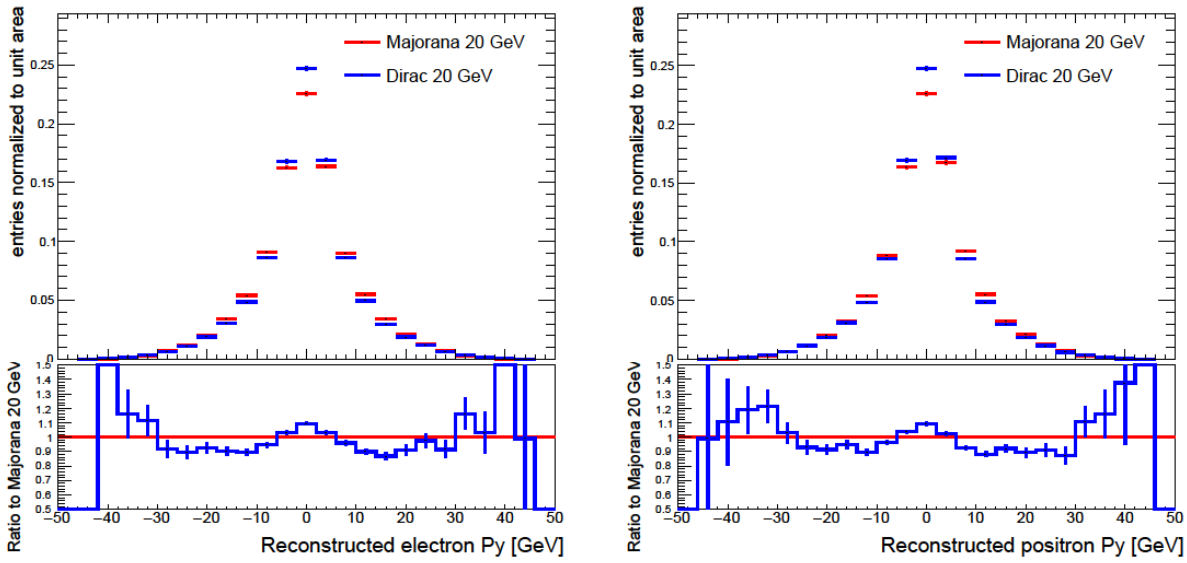

Fig. 5.8a (left): p_y distribution of final state electrons, Fig. 5.8b(right): p_y distribution of final state positrons

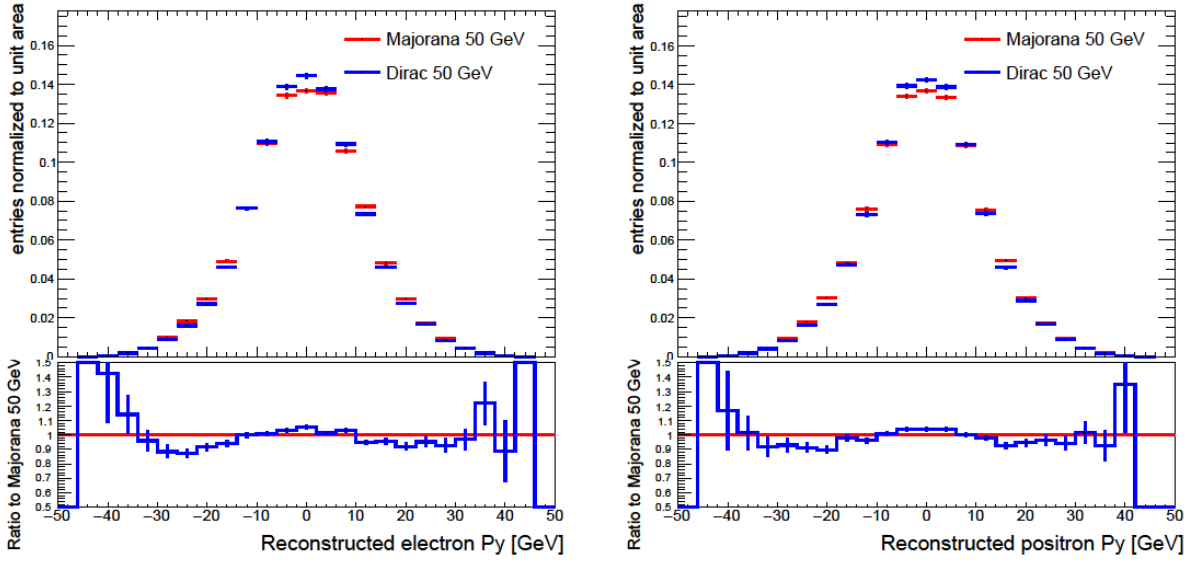

Fig. 5.9a (left): p_y distribution of final state electrons, Fig. 5.9b(right): p_y distribution of final state positrons

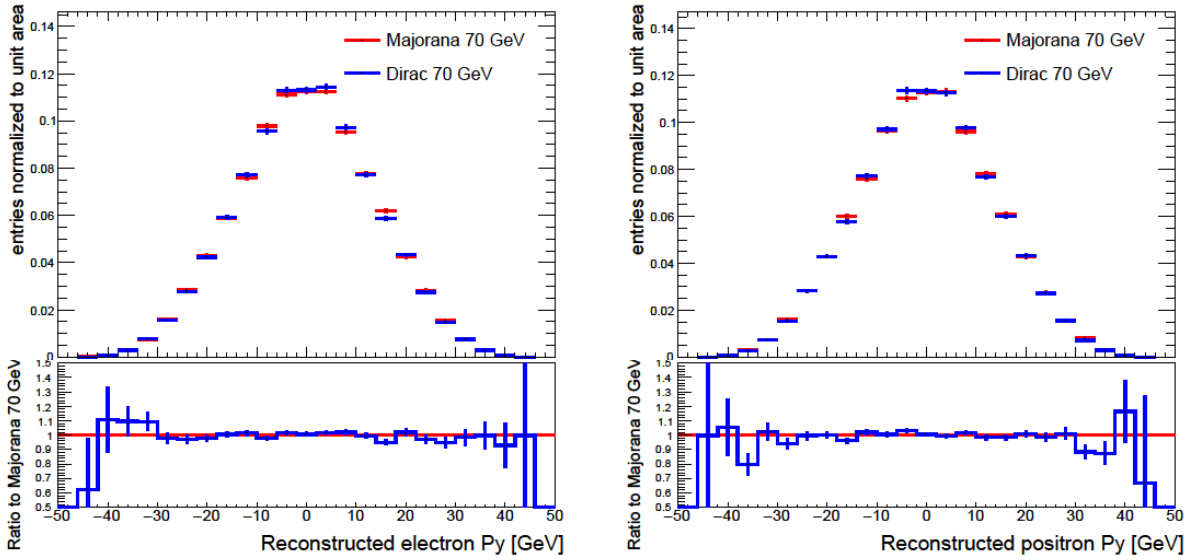

Fig. 5.10a (left): p_y distribution of final state electrons, Fig. 5.10b(right): p_y distribution of final state positrons

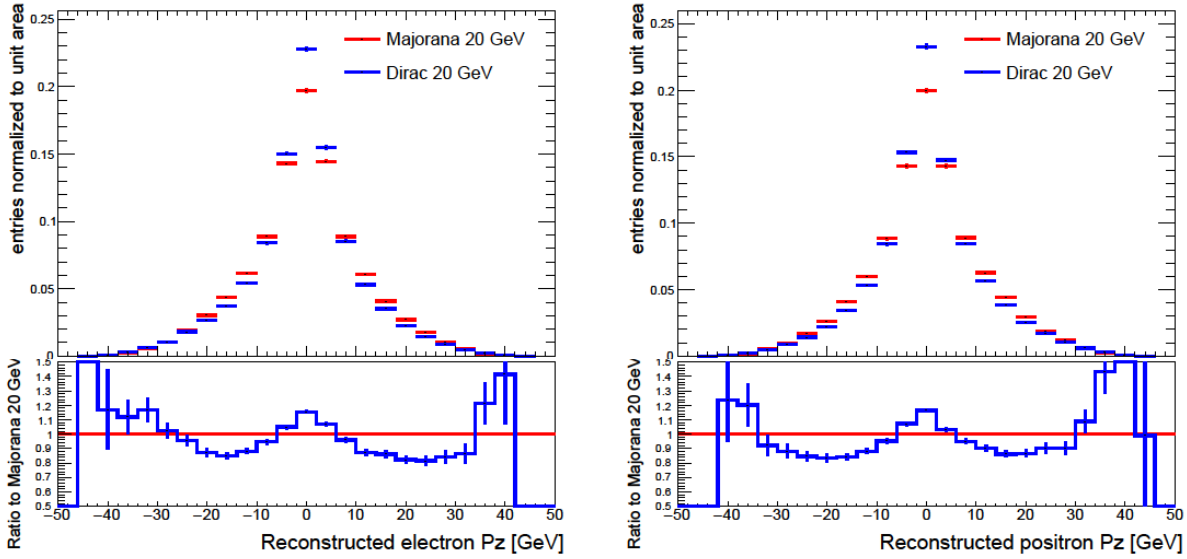

Fig. 5.11a (left): p_z distribution of final state electrons, Fig. 5.11b(right): p_z distribution of final state positrons

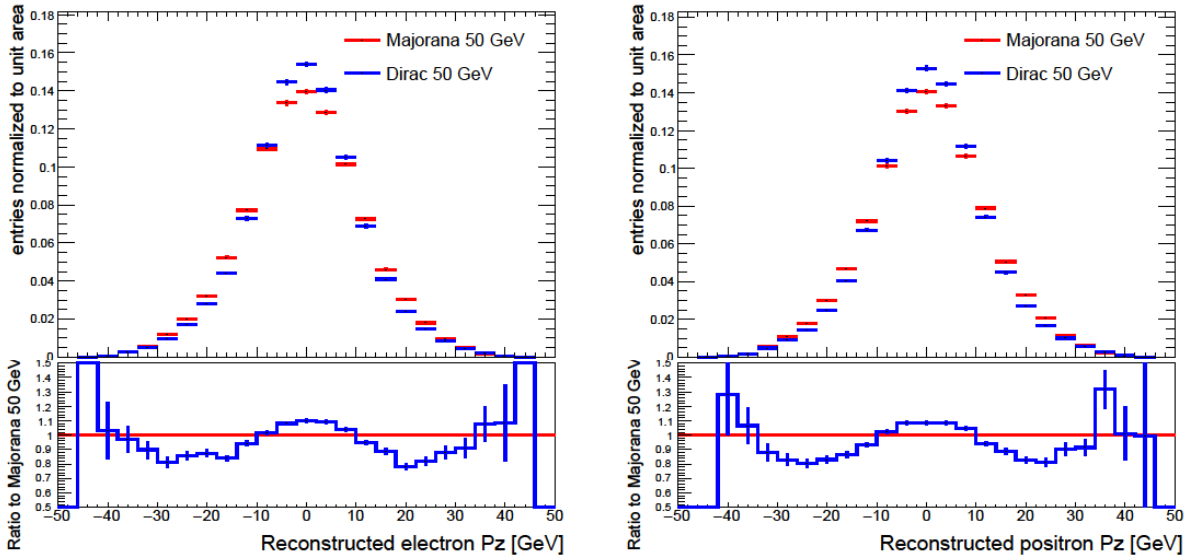

Fig. 5.12a (left): p_z distribution of final state electrons, Fig. 5.12b(right): p_z distribution of final state positrons

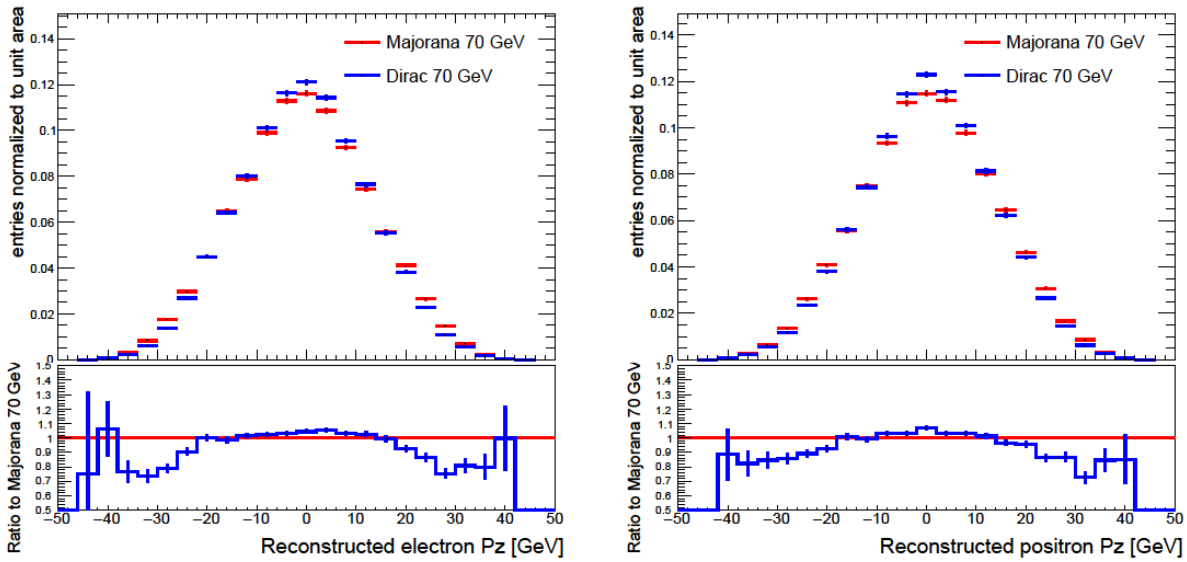

Fig. 5.13a (left): p_z distribution of final state electrons, Fig. 5.13b(right): p_z distribution of final state positrons

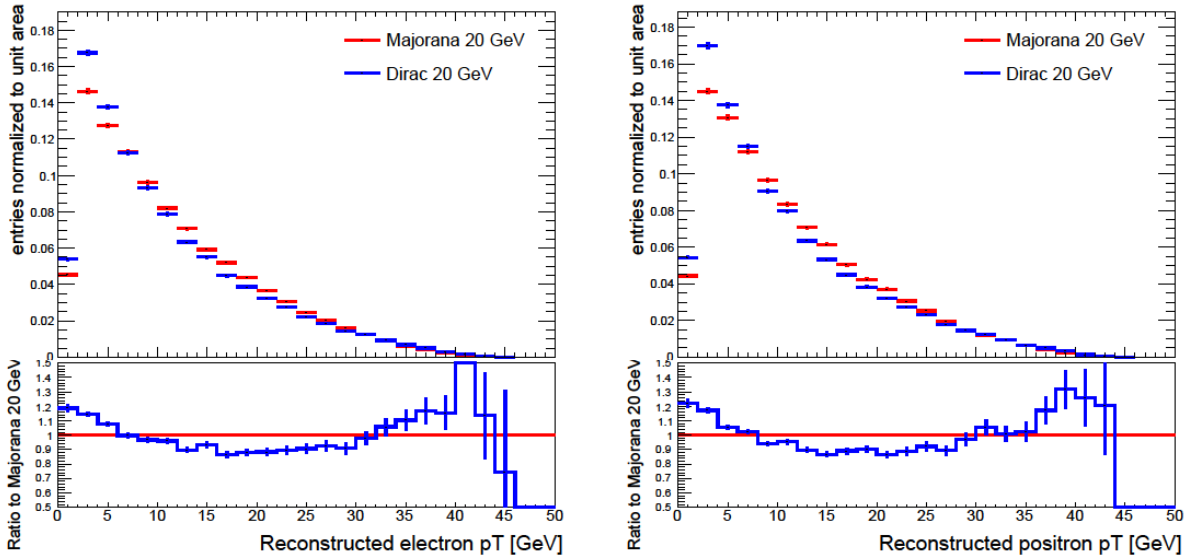

Fig. 5.14a (left): pT distribution of final state electrons, Fig. 5.14b(right): pT distribution of final state positrons

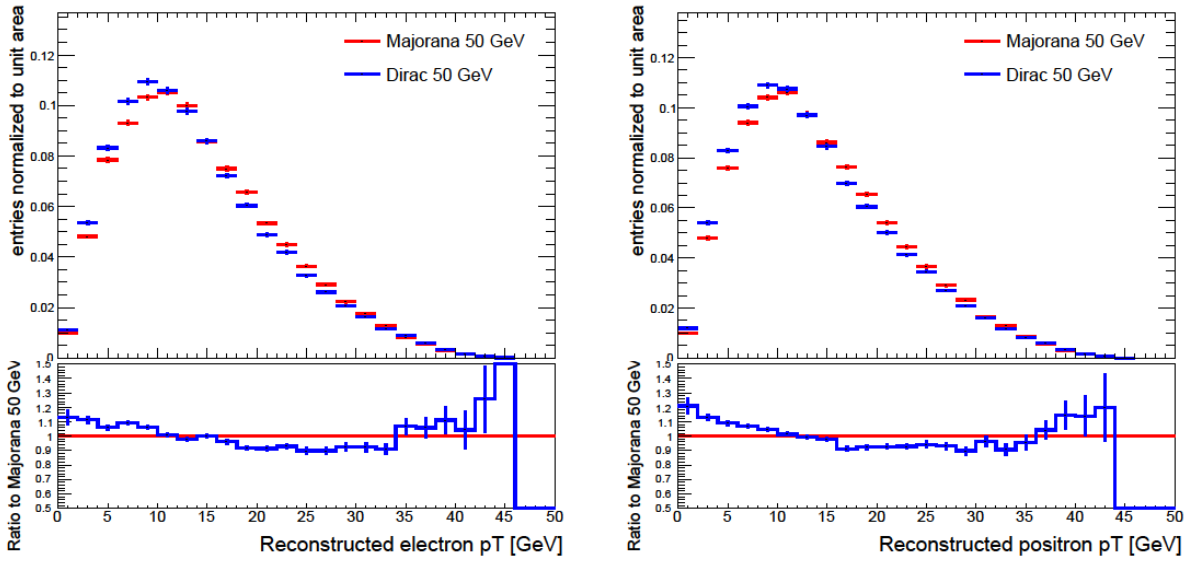

Fig. 5.15a (left): pT distribution of final state electrons, Fig. 5.15b(right): pT distribution of final state positrons

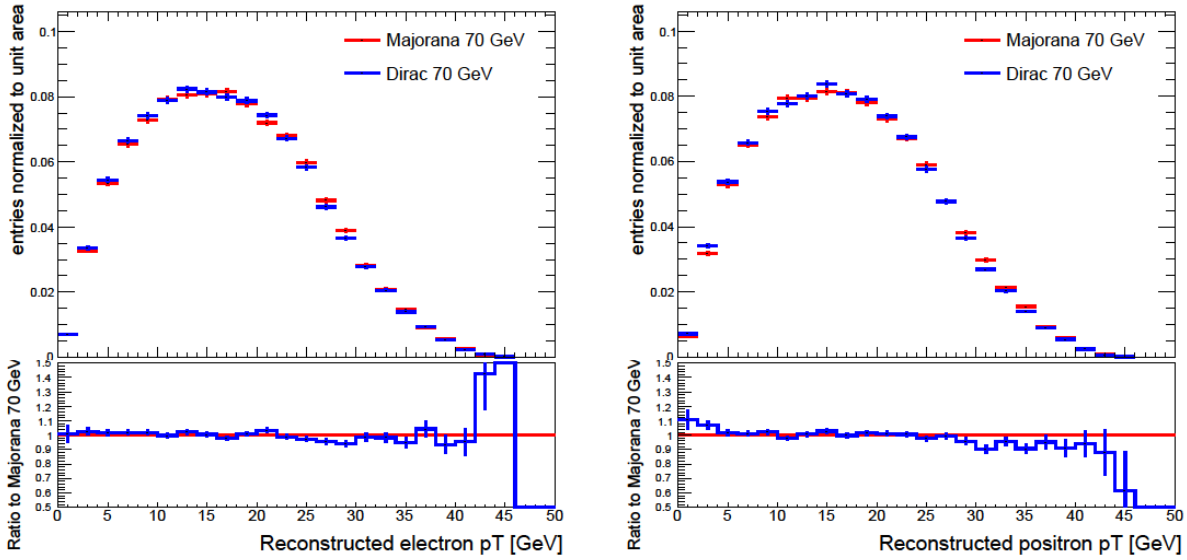

Fig. 5.16a (left): pT distribution of final state electrons, Fig. 5.16b(right): pT distribution of final state positrons

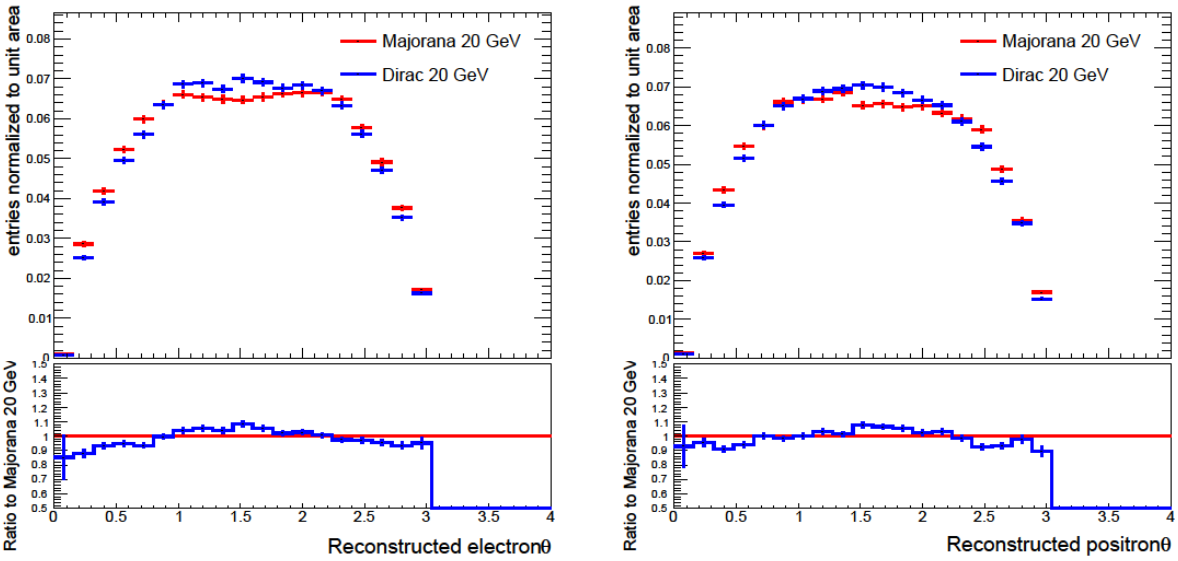

Fig. 5.17a (left): θ distribution of final state electrons, Fig. 5.17b(right): θ distribution of final state positrons

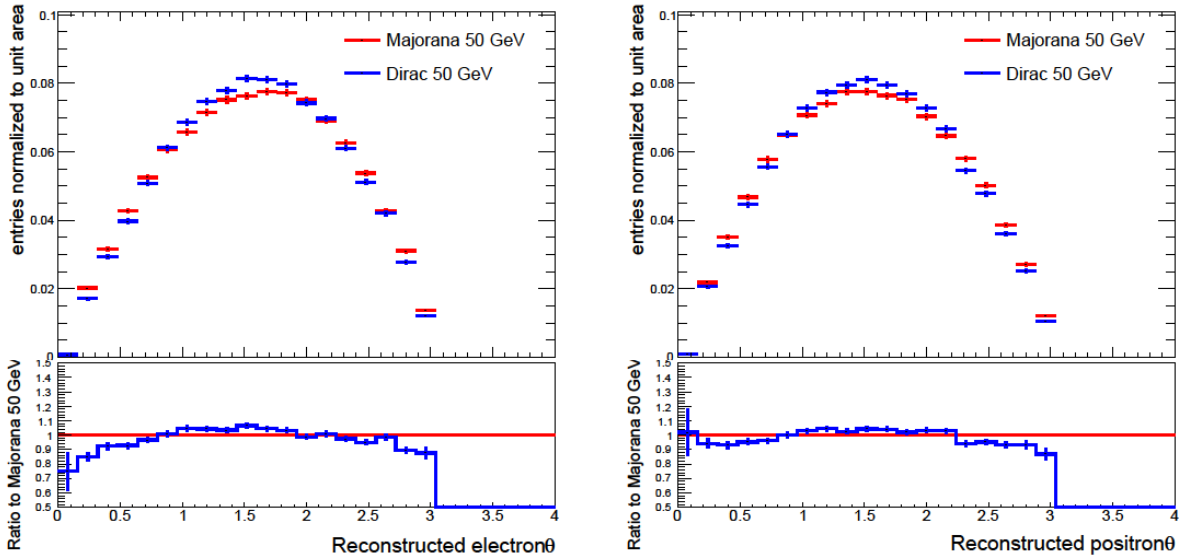

Fig. 5.18a (left): θ distribution of final state electrons, Fig. 5.18b(right): θ distribution of final state positrons

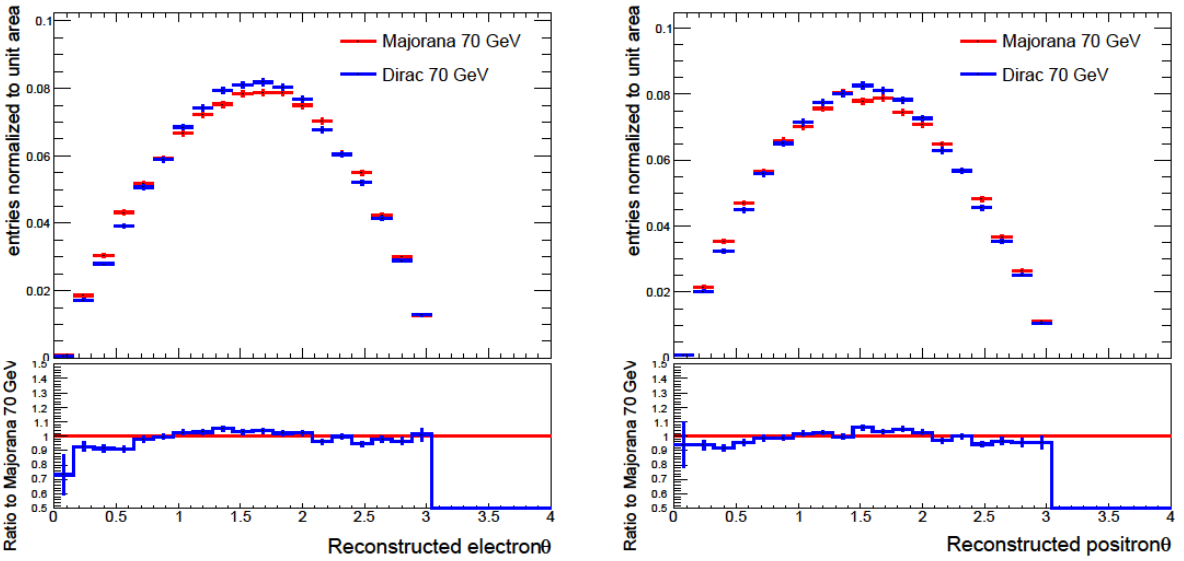

Fig. 5.19a (left): θ distribution of final state electrons, Fig. 5.19b(right): θ distribution of final state positrons

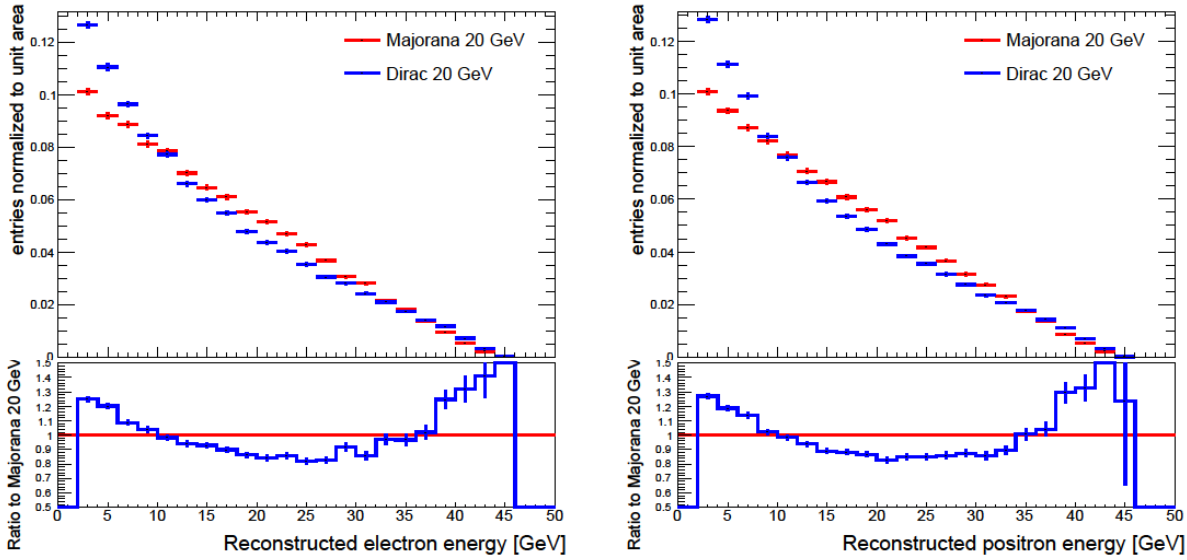

Fig. 5.20a (left): E distribution of final state electrons, Fig. 5.20b(right): E distribution of final state positrons

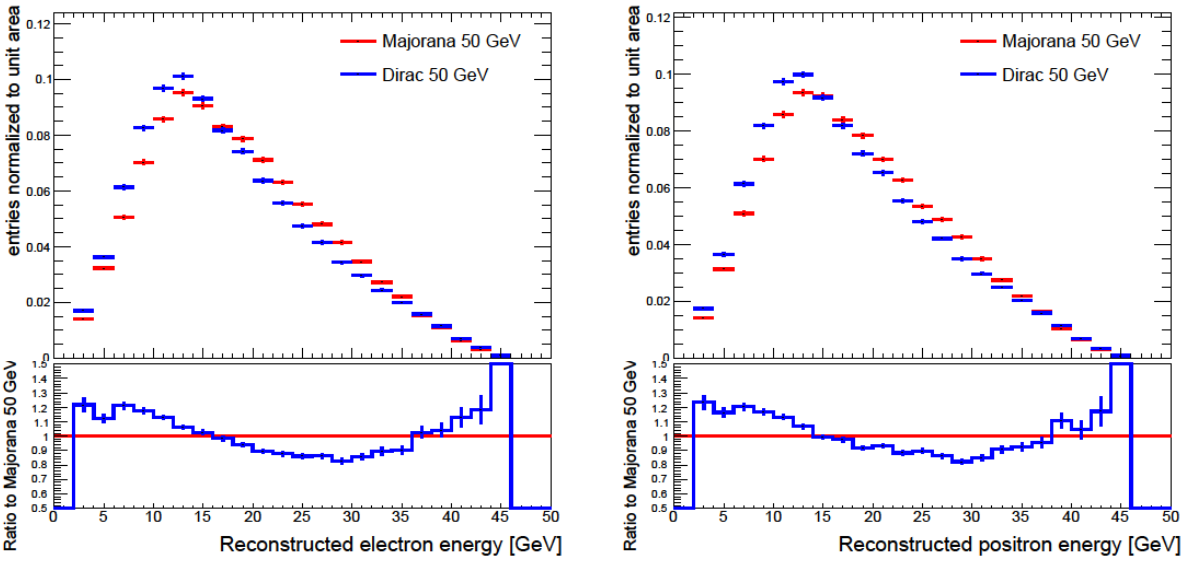

Fig. 5.21a (left): E distribution of final state electrons, Fig. 5.21b(right): E distribution of final state positrons

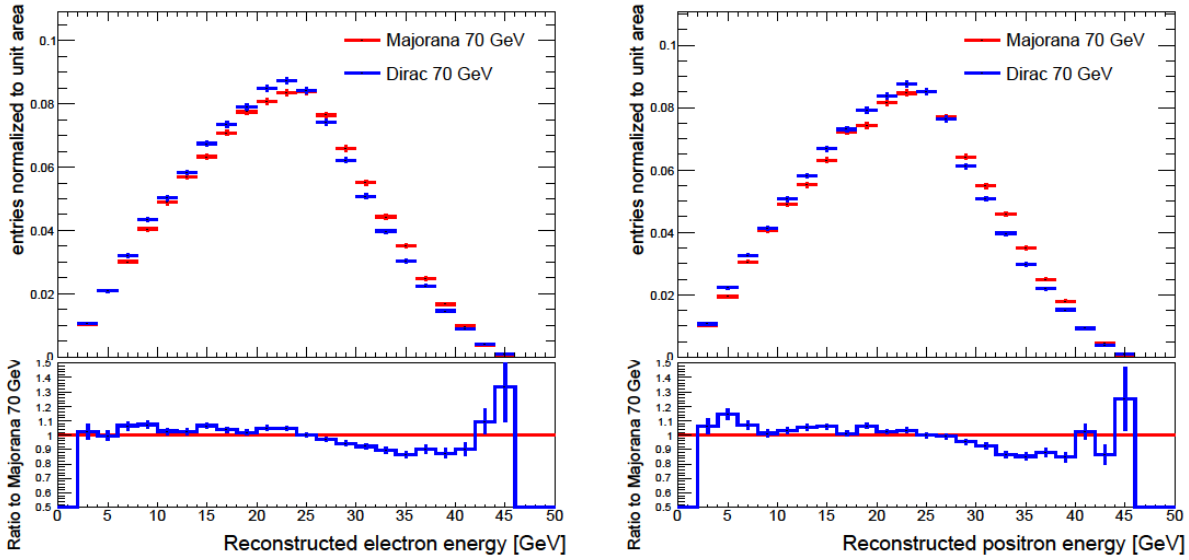

Fig. 5.22a (left): E distribution of final state electrons, Fig. 5.22b(right): E distribution of final state positrons

All the variables shown above, p_x (Fig. 5.5 – 5.7), p_y (Fig. 5.8 – 5.10), p_z (Fig. 5.11 – 5.13), pT (Fig. 5.14 – 5.16), θ (Fig. 5.17 – 5.19), and E (Fig. 5.20 – 5.22) demonstrate two key features:

1. All the variables show Dirac vs Majorana distinction, however these distinctions have some oscillatory (as seen in ratio plots) behavior to them (its importance is explained below)
2. The distinctions tend to decrease as the mass of the HNL tends to W boson mass

The 2nd feature is not expected, as in general, the Dirac Majorana Confusion Theorem [18] states that differences between Dirac and Majorana are proportional to their masses, and hence it was expected that these differences should only increase (very slightly in this case, as the order of magnitude is the same) or stay the same. As of the writing of this thesis, I do not know the reason for the observations made above and it is therefore an open question to be looked at in future studies, specifically in the context of whether a certain step in the

simulation process makes some simplifications or assumptions that would be true for lighter HNLs and not for heavier HNLs.

The 1st feature regarding the distinctions between the variables of final state leptons is only clearly visible at significantly large statistics. To put statistics size requirement into perspective, it is worth noting that in [17], in Sec. 3.2.3, where results from this project were briefly described, these variables were not at all mentioned because these differences were not observed (or they were observed to be smaller than statistical error bars). During the stage of writing of [17], the number of total Monte Carlo generated events (before any selections) was 10'000. The analysis shown in the thesis here corresponds to 100'000 Monte Carlo generated events (before any selections). This suggests that these variables are indeed able to distinguish between the Dirac and Majorana nature (as expected because they are directly or indirectly related to angular distribution), however they require a significantly higher sample size. It is proposed that further explorations of these variables be done using Deep Neural Networks or some other modern Machine Learning techniques which could be used to develop classifiers that work more efficiently and are thus able to distinguish between the Dirac vs Majorana nature with a smaller sample size.

The next two variables to look at are the lifetime and transverse distance of the displaced vertex. These are natural choices for long lived particles. Here it needs to be noted that this analysis was performed for a mixing angle of 1e-3, which has a direct impact on these two variables. This mixing angle is expected to give $\mathcal{O}(1e4)$ events for 50 GeV particle as shown in Table 4.1. The choice of mixing angle was based on the number of expected events which

in turn was chosen due to the choice of the main variables of distinction in this study (explained later below).

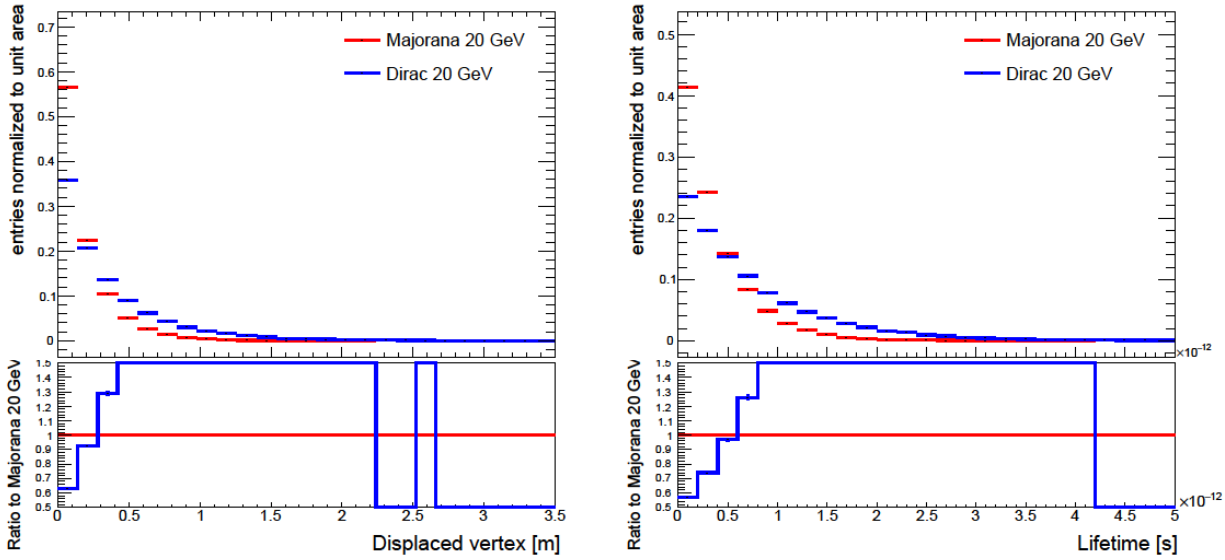

Fig. 5.23 (left): Distance between beam axis and displaced vertex, Fig. 5.24 (right): Lifetime of HNL

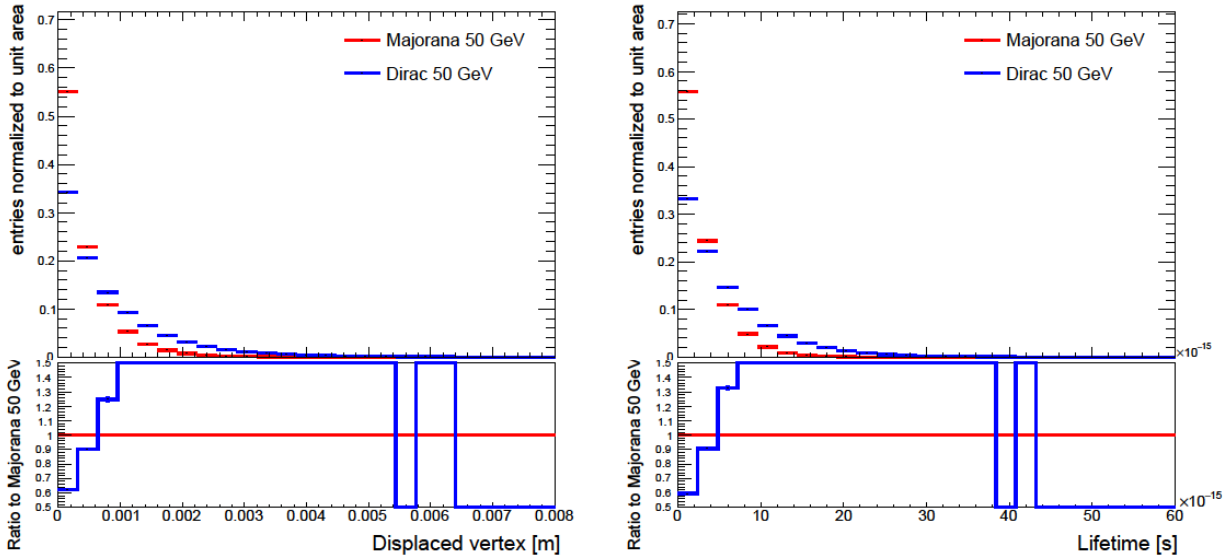

Fig. 5.25 (left): Distance between beam axis and displaced vertex, Fig. 5.26 (right): Lifetime of HNL

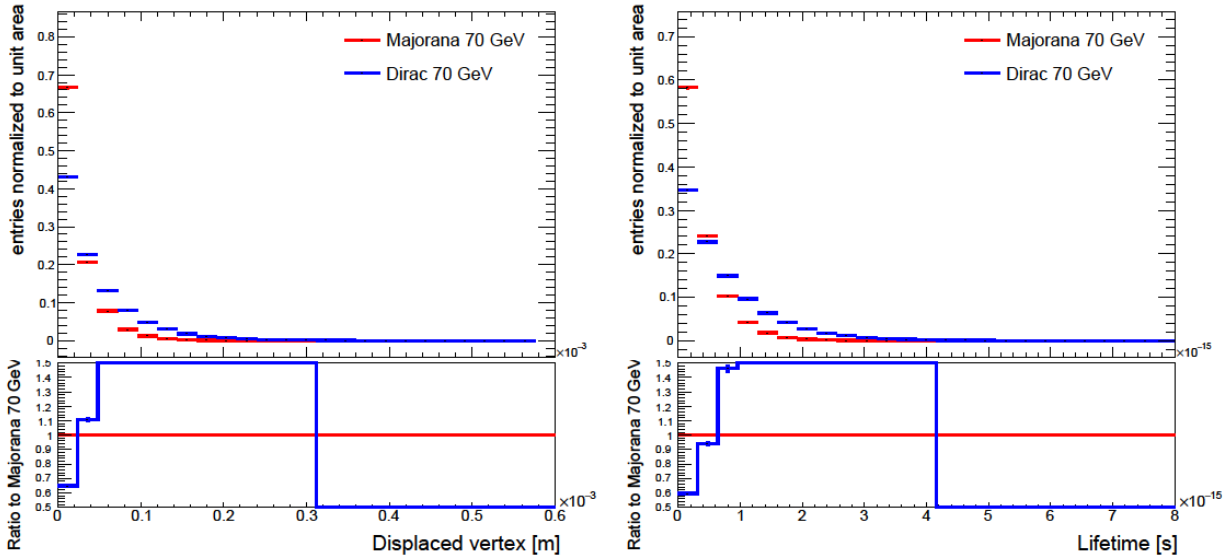

Fig. 5.27 (left): Distance between beam axis and displaced vertex, Fig. 5.28 (right): Lifetime of HNL

These two variables, the displaced vertex distance and the lifetime are the clearest variables that allow for the distinction between the Dirac vs Majorana case, however to identify the nature of HNL, the mass and the mixing angle have to be known exactly. Therefore, these variables can not be used on their own for the purposes of distinction. In a real experiment, the reconstructed mass of the HNL and the cross section measurements (that can provide the mixing angles) could allow for these variables to provide a clear distinction. A detailed explanation for this can be found in [17] Sec. 3.2.3.

The next two variables of focus are the missing transverse energy and the angle between the final state electron and positron (θ_{ee}).

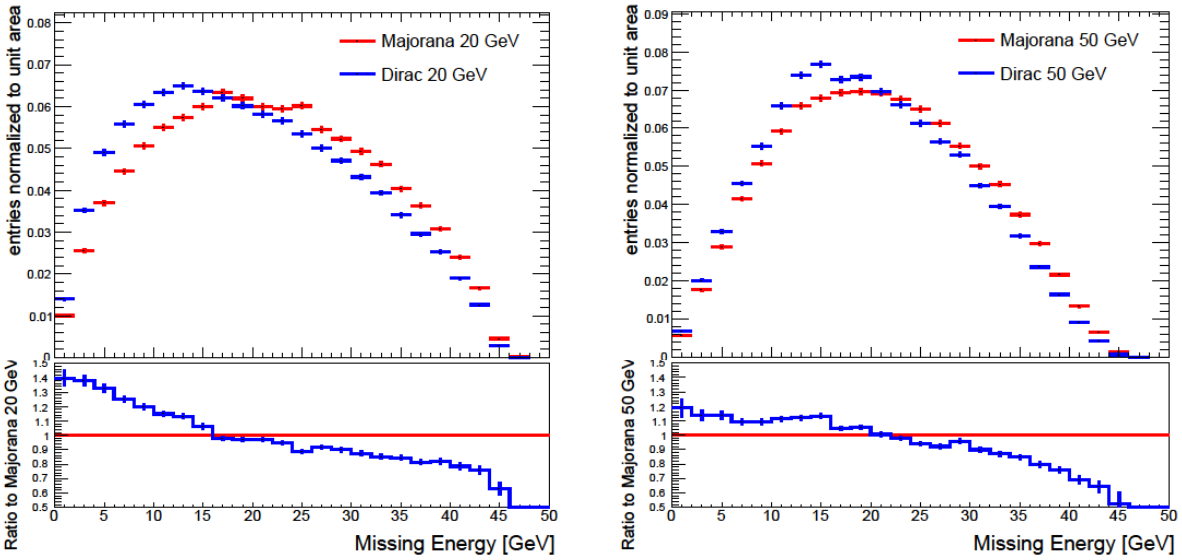

Fig. 5.29 (left) and Fig. 5.30 (right): Missing Energy

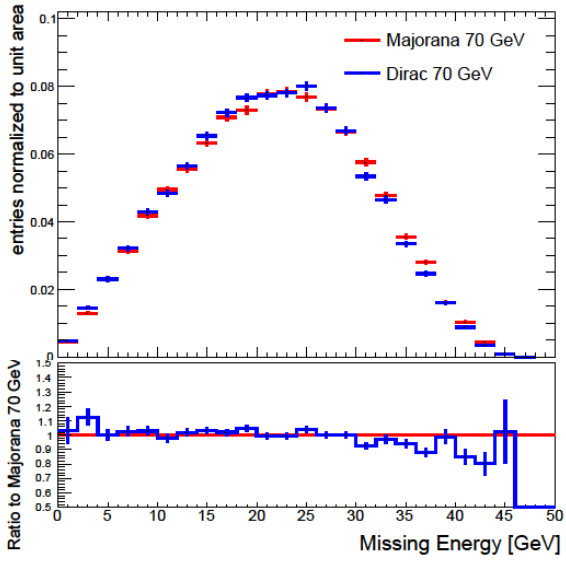

Fig. 5.31: Missing Energy

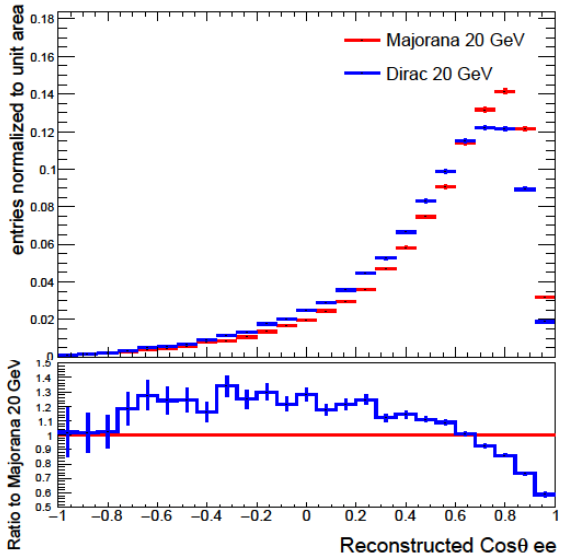

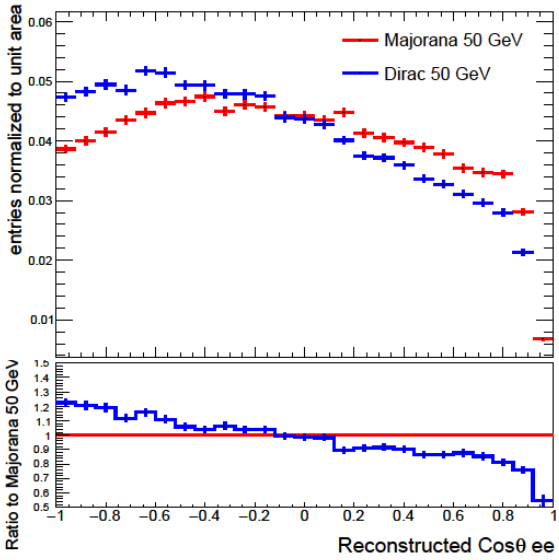

Fig. 5.32 (left) and Fig. 5.33 (right): Reconstructed cos θ_{ee}

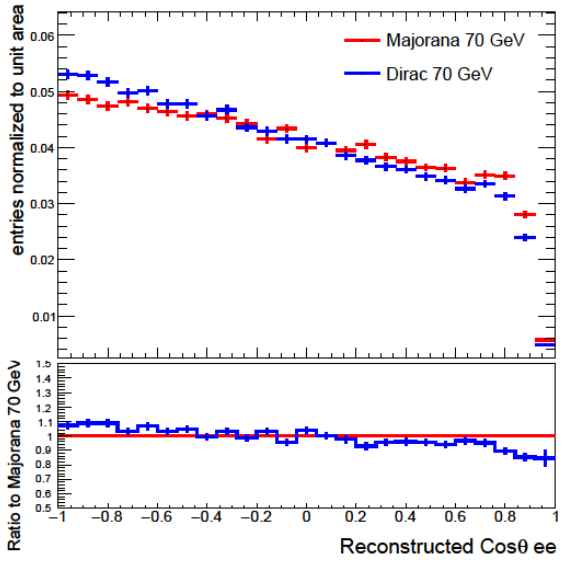

Fig. 5.34: Reconstructed cos θ_{ee}

The missing transverse energy variable corresponds to the energy in the perpendicular plane that isn't detected in the experiment but should be present due to the conservation of

energy. In this analysis, it corresponds to the transverse energy that is not picked up by the detectors as it is carried by the 2 neutrinos/anti neutrinos that escape the detectors undetected. This variable seems to provide a much cleaner distinction as the ratio of Dirac to Majorana HNL has a very linear trend whereby at 0 GeV, it is maximum, at a quarter of the total center of mass energy, it is 1 and at a half of the total center of mass energy, it is at its minimum.

The cos θ_{ee} variable, which is the cosine of the angle between the final state electron and positron provides the clearest distinction between the Dirac vs Majorana HNLs. Initially this analysis was performed at a no. of events of the order of $\mathcal{O}(1e3)$. Cos θ_{ee} was able to show the Dirac vs Majorana distinction but the distinction was not as clear as above. In the next iteration, the analysis was performed at $\mathcal{O}(1e4)$ no. of events. This is when this particular variable provided a very clearly visible distinction. This motivated the choice for the analysis to be done on HNLs with mixing angle of 1e-3, which if such an HNL with such a mixing angle exists, should provide roughly $\mathcal{O}(1e4)$ no. of events at the proposed Tera Z factory run of the FCC-ee. Cos θ_{ee} could allow for a distinction for mixing angles of 1e-3 and above directly for HNLs with a mass above 30-40 GeV. For HNLs below that mass, the number of events will have reduced potentially making the distributions not as clear, however for these masses with a little larger mixing angle, such as an HNL with 20 GeV mass and 1e-2 mixing angle, it is still possible to carry such an analysis. For mixing angles below 1e-3, it may still be possible to make the distinction by employing advanced machine learning techniques.

The features of the cos(θ_{ee}) variable to notice are that:

- $\cos(\theta_{ee})$ distribution of the Dirac HNL has a higher number of events for larger angles compared to Majorana HNL
- Conversely, $\cos(\theta_{ee})$ distribution of the Majorana HNL has a higher number of events for smaller angles compared to the Dirac HNL
- The value of $\cos(\theta_{ee})$ at which Majorana distribution becomes higher in value than Dirac distribution seems to reduce as the mass of the HNL increases, or more simply, the angle, at which the ratio cross over happens, increases as the mass of the HNL increases.
- The shape of the distribution for different masses varies widely due to the fact that all HNLs are produced at a center of mass energy of ~ 91 GeV, and hence the boost of the HNL will vary with their masses. For particle systems that are boosted, the angles between final state particles are reduced, hence in the above distribution, lighter HNLs (which are boosted more heavily) have higher no. of events involving smaller values of θ_{ee}.

With this, the experimental section of this thesis comes to an end. In the next section, the entire project is concluded with a comparison between the results obtained from the theoretical and experimental parts of my thesis.

Chapter 6: Summary and Conclusion

In this thesis, heavy neutral leptons, which are hypothesized heavy mass eigenstates of neutrinos that provide mass mechanisms for neutrinos, were explored. In particular, they were studied within the context of Type I Seesaw and Inverse Seesaw models, which propose the existence of Majorana and Dirac HNLs respectively. If sterile heavy neutral leptons indeed exist, it would be an imperative task to ascertain their Majorana or Dirac nature as that would provide a statement on whether lepton number is conserved in nature. In this thesis, the distinction between the Dirac vs Majorana nature is explored. The leptonic decay channels were explored to find kinematical observables that can discriminate between Dirac vs Majorana nature of the HNL. In particular, this was done through two methods:

1. Theoretically, by performing differential decay width computations through the use of helicity amplitudes
2. Phenomenologically, by MC event generation, detector simulations and analysis within the FCC-ee framework

The results obtained for 20, 50 and 70 GeV HNLs are as shown below for comparison:

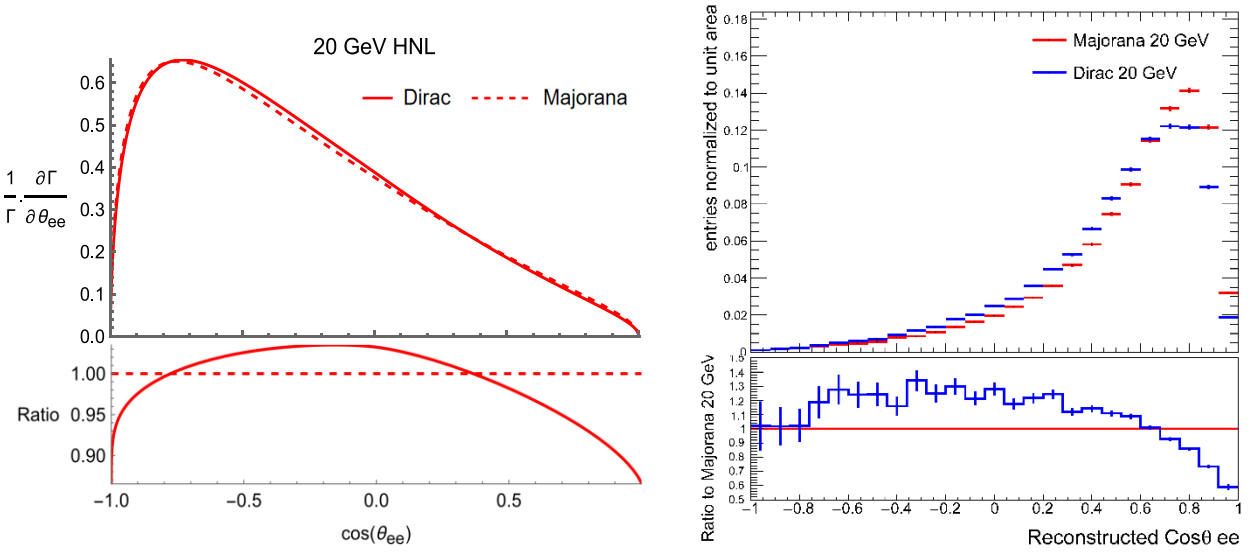

Fig. 6.1a (left): Theoretical cos θ_{ee} distribution, and Fig. 6.1b (right): Experimental cos θ_{ee} distribution for a 20 GeV HNL

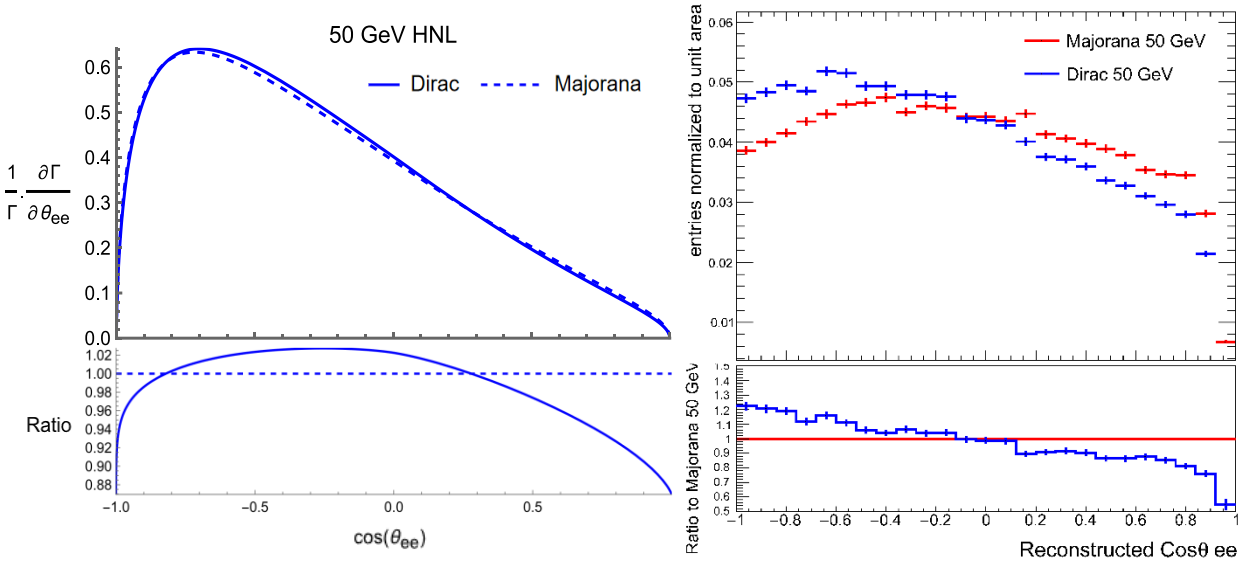

Fig. 6.2a (left): Theoretical cos θ_{ee} distribution, and Fig. 6.2b (right): Experimental cos θ_{ee} distribution for a 50 GeV HNL

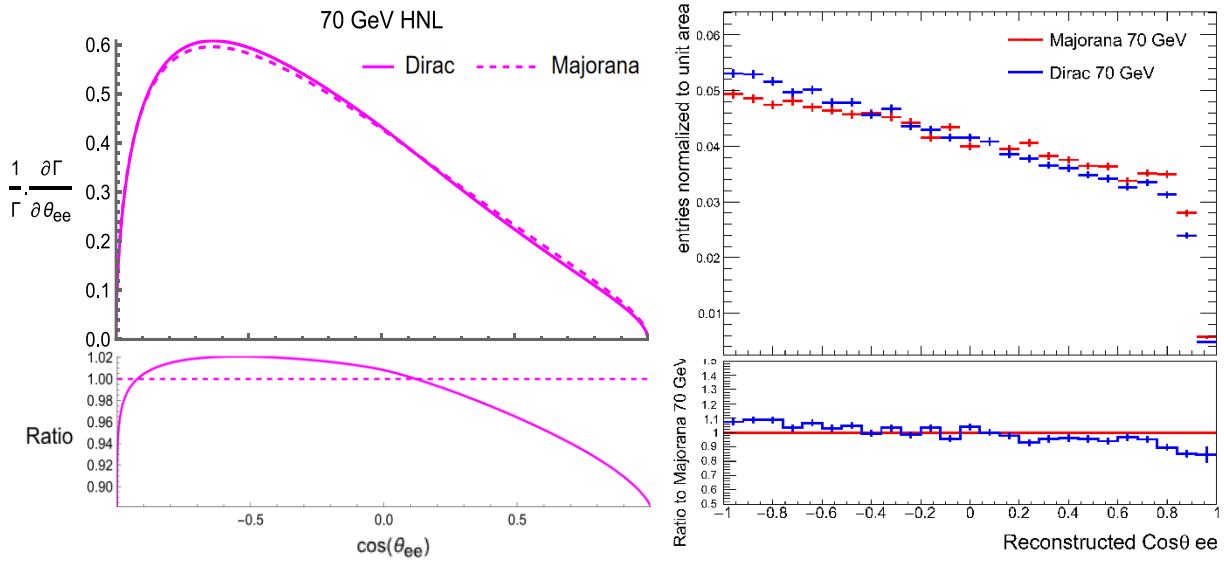

Fig. 6.3a (left): Theoretical cos θ_{ee} distribution, and Fig. 6.3b (right): Experimental cos θ_{ee} distribution for a 70 GeV HNL

The results appear to be mostly consistent:

- Dirac distribution > Majorana distribution for larger θ_{ee}
- Majorana distribution > Dirac distribution for smaller θ_{ee}
- As HNL mass increases, the value of θ_{ee} at which Dirac and Majorana distribution cross over also increases

There is some inconsistency in the theoretical and experimental plots in the $\cos(\theta_{ee})$ range from -1 to -0.8, however, these ranges denote the largest angles of separation, which would have the highest difference in the rest frame vs laboratory (boosted) frame of reference.

The same can be said about the difference in the shape of the distribution between the theoretical and experimental plots which is as expected, as theoretical plots correspond to θ_{ee} in the HNL's center of mass frame whereas the experimental plots correspond to θ_{ee} in the laboratory frame, whereby the lighter the HNL, the more boosted the final state particles. For example, for the 20 GeV HNL, in the experimental plots (laboratory frame), the distribution peaks for particles that have small angular separation as opposed to the theoretical plots (center of mass frame) where the distribution peaks when the particles are back to back.

Appendix A

The appendix shows the entire Mathematica code that was written for theoretical computation done for this project. The computations were run on the University of Geneva's high performance Baobab cluster.

HNL amplitude and differential decay width calculations

```
In[•]:= g0 = ({{1, 0, 0, 0}, {0, 1, 0, 0}, {0, 0, -1, 0}, {0, 0, 0, -1}});
g1 = ({{0, 0, 0, 1}, {0, 0, 1, 0}, {0, -1, 0, 0}, {-1, 0, 0, 0}});
g2 = ({{0, 0, 0, -I}, {0, 0, I, 0}, {0, I, 0, 0}, {-I, 0, 0, 0}});
g3 = ({{0, 0, 1, 0}, {0, 0, 0, -1}, {-1, 0, 0, 0}, {0, 1, 0, 0}});
g5 = I * (g0.g1.g2.g3);
PL = (1 / 2) * (IdentityMatrix[4] - g5);
PR = (1 / 2) * (IdentityMatrix[4] + g5);
Peez = ({{(-1 / 2) + (2 * Sin[thetaW] * Sin[thetaW]), 0, 1 / 2, 0},
    {0, (-1 / 2) + (2 * Sin[thetaW] * Sin[thetaW]), 0, 1 / 2},
    {1 / 2, 0, (-1 / 2) + (2 * Sin[thetaW] * Sin[thetaW]), 0},
    {0, 1 / 2, 0, (-1 / 2) + (2 * Sin[thetaW] * Sin[thetaW])}});
MT = ({{1, 0, 0, 0}, {0, -1, 0, 0}, {0, 0, -1, 0}, {0, 0, 0, -1}});

In[•]:= S1D1L = ({{0, 0, 0, -√(2 * mN)}});
S2D1L = ({{(√(pV)) (Sin[thetaV / 2])}, {-(√(pV)) (E^(I * phiV)) (Cos[thetaV / 2])},
    {-(√(pV)) (Sin[thetaV / 2])}, {(√(pV)) (E^(I * phiV)) (Cos[thetaV / 2])}});
S3D1L = ({{-(√(pE)) (Sin[thetaE / 2]), (√(pE)) (E^(-I * phiE)) (Cos[thetaE / 2]),
     -(√(pE)) (Sin[thetaE / 2]), (√(pE)) (E^(-I * phiE)) (Cos[thetaE / 2])}});
S4D1L = ({{(√(pP)) (Sin[thetaP / 2])}, {-(√(pP)) (E^(I * phiP)) (Cos[thetaP / 2])},
    {-(√(pP)) (Sin[thetaP / 2])}, {(√(pP)) (E^(I * phiP)) (Cos[thetaP / 2])}});
J1D1L = ({{(S1D1L.g0.PL.S2D1L)[[1, 1]]}, {(S1D1L.g1.PL.S2D1L)[[1, 1]]},
    {(S1D1L.g2.PL.S2D1L)[[1, 1]]}, {(S1D1L.g3.PL.S2D1L)[[1, 1]]}});
J2D1L = ({{(S3D1L.g0.Peez.S4D1L)[[1, 1]]}, {(S3D1L.g1.Peez.S4D1L)[[1, 1]]},
    {(S3D1L.g2.Peez.S4D1L)[[1, 1]]}, {(S3D1L.g3.Peez.S4D1L)[[1, 1]]}});
MD1L = (J1D1L^T.MT.J2D1L)[[1, 1]] // Simplify;
MD1LC = MD1L /. {I → -I, -I → I};
MD1L = MD1L * (I * g^2) / (4 * Cos[thetaW]^2 * (mN^2 - 2 * mN * pV - mZ^2)) // Simplify;
MD1LC = MD1LC * (-I * g^2) / (4 * Cos[thetaW]^2 * (mN^2 - 2 * mN * pV - mZ^2)) // Simplify;
S1D1R = ({{0, 0, 0, -√(2 * mN)}});
S2D1R = ({{(√(pV)) (Sin[thetaV / 2])}, {-(√(pV)) (E^(I * phiV)) (Cos[thetaV / 2])},
    {-(√(pV)) (Sin[thetaV / 2])}, {(√(pV)) (E^(I * phiV)) (Cos[thetaV / 2])}});
S3D1R = ({{(√(pE)) (Cos[thetaE / 2]), (√(pE)) (E^(-I * phiE)) (Sin[thetaE / 2]),
     -(√(pE)) (Cos[thetaE / 2]), -(√(pE)) (E^(-I * phiE)) (Sin[thetaE / 2])}});
S4D1R = ({{(√(pP)) (Cos[thetaP / 2])}, {(√(pP)) (E^(I * phiP)) (Sin[thetaP / 2])},
    {(√(pP)) (Cos[thetaP / 2])}, {(√(pP)) (E^(I * phiP)) (Sin[thetaP / 2])}});
J1D1R = ({{(S1D1R.g0.PL.S2D1R)[[1, 1]]}, {(S1D1R.g1.PL.S2D1R)[[1, 1]]},
    {(S1D1R.g2.PL.S2D1R)[[1, 1]]}, {(S1D1R.g3.PL.S2D1R)[[1, 1]]}});
J2D1R = ({{(S3D1R.g0.Peez.S4D1R)[[1, 1]]}, {(S3D1R.g1.Peez.S4D1R)[[1, 1]]},
    {(S3D1R.g2.Peez.S4D1R)[[1, 1]]}, {(S3D1R.g3.Peez.S4D1R)[[1, 1]]}});
MD1R = (J1D1R^T.MT.J2D1R)[[1, 1]] // Simplify;
MD1RC = MD1R /. {I → -I, -I → I};
MD1R = MD1R * (I * g^2) / (4 * Cos[thetaW]^2 * (mN^2 - 2 * mN * pV - mZ^2)) // Simplify;
MD1RC = MD1RC * (-I * g^2) / (4 * Cos[thetaW]^2 * (mN^2 - 2 * mN * pV - mZ^2)) // Simplify;
```

```
S1D2L = ({{0, 0, -√(2 * mN), 0}});
S2D2L = ({{(√(pV)) (Cos[thetaV / 2])}, {(√(pV)) (E^(I * phiV)) (Sin[thetaV / 2])},
    {(√(pV)) (Cos[thetaV / 2])}, {(√(pV)) (E^(I * phiV)) (Sin[thetaV / 2])}});
S3D2L = ({{-(√(pE)) (Sin[thetaE / 2]), (√(pE)) (E^(-I * phiE)) (Cos[thetaE / 2]),
     -(√(pE)) (Sin[thetaE / 2]), (√(pE)) (E^(-I * phiE)) (Cos[thetaE / 2])}});
S4D2L = ({{(√(pP)) (Sin[thetaP / 2])}, {-(√(pP)) (E^(I * phiP)) (Cos[thetaP / 2])},
    {-(√(pP)) (Sin[thetaP / 2])}, {(√(pP)) (E^(I * phiP)) (Cos[thetaP / 2])}});
J1D2L = ({{-(S1D2L.g0.PR.S2D2L)[[1, 1]]}, {-(S1D2L.g1.PR.S2D2L)[[1, 1]]},
    {-(S1D2L.g2.PR.S2D2L)[[1, 1]]}, {-(S1D2L.g3.PR.S2D2L)[[1, 1]]}});
J2D2L = ({{(S3D2L.g0.Peez.S4D2L)[[1, 1]]}, {(S3D2L.g1.Peez.S4D2L)[[1, 1]]},
    {(S3D2L.g2.Peez.S4D2L)[[1, 1]]}, {(S3D2L.g3.Peez.S4D2L)[[1, 1]]}});
MD2L = (J1D2L^T.MT.J2D2L)[[1, 1]] // Simplify;
MD2LC = MD2L /. {I → -I, -I → I};
MD2L = MD2L * (I * g^2) / (4 * Cos[thetaW]^2 * (mN^2 - 2 * mN * pV - mZ^2)) // Simplify;
MD2LC = MD2LC * (-I * g^2) / (4 * Cos[thetaW]^2 * (mN^2 - 2 * mN * pV - mZ^2)) // Simplify;
S1D2R = ({{0, 0, -√(2 * mN), 0}});
S2D2R = ({{(√(pV)) (Cos[thetaV / 2])}, {(√(pV)) (E^(I * phiV)) (Sin[thetaV / 2])},
    {(√(pV)) (Cos[thetaV / 2])}, {(√(pV)) (E^(I * phiV)) (Sin[thetaV / 2])}});
S3D2R = ({{(√(pE)) (Cos[thetaE / 2]), (√(pE)) (E^(-I * phiE)) (Sin[thetaE / 2]),
     -(√(pE)) (Cos[thetaE / 2]), -(√(pE)) (E^(-I * phiE)) (Sin[thetaE / 2])}});
S4D2R = ({{(√(pP)) (Cos[thetaP / 2])}, {(√(pP)) (E^(I * phiP)) (Sin[thetaP / 2])},
    {(√(pP)) (Cos[thetaP / 2])}, {(√(pP)) (E^(I * phiP)) (Sin[thetaP / 2])}});
J1D2R = ({{-(S1D2R.g0.PR.S2D2R)[[1, 1]]}, {-(S1D2R.g1.PR.S2D2R)[[1, 1]]},
    {-(S1D2R.g2.PR.S2D2R)[[1, 1]]}, {-(S1D2R.g3.PR.S2D2R)[[1, 1]]}});
J2D2R = ({{(S3D2R.g0.Peez.S4D2R)[[1, 1]]}, {(S3D2R.g1.Peez.S4D2R)[[1, 1]]},
    {(S3D2R.g2.Peez.S4D2R)[[1, 1]]}, {(S3D2R.g3.Peez.S4D2R)[[1, 1]]}});
MD2R = (J1D2R^T.MT.J2D2R)[[1, 1]] // Simplify;
MD2RC = MD2R /. {I → -I, -I → I};
MD2R = MD2R * (I * g^2) / (4 * Cos[thetaW]^2 * (mN^2 - 2 * mN * pV - mZ^2)) // Simplify;
MD2RC = MD2RC * (-I * g^2) / (4 * Cos[thetaW]^2 * (mN^2 - 2 * mN * pV - mZ^2)) // Simplify;
S1D3L = ({{-(√(pV)) (Sin[thetaV / 2]), (√(pV)) (E^(-I * phiV)) (Cos[thetaV / 2]),
     -(√(pV)) (Sin[thetaV / 2]), (√(pV)) (E^(-I * phiV)) (Cos[thetaV / 2])}});
S2D3L = ({{0}, {√(2 * mN)}, {0}, {0}});
S3D3L = ({{-(√(pE)) (Sin[thetaE / 2]), (√(pE)) (E^(-I * phiE)) (Cos[thetaE / 2]),
     -(√(pE)) (Sin[thetaE / 2]), (√(pE)) (E^(-I * phiE)) (Cos[thetaE / 2])}});
S4D3L = ({{(√(pP)) (Sin[thetaP / 2])}, {-(√(pP)) (E^(I * phiP)) (Cos[thetaP / 2])},
    {-(√(pP)) (Sin[thetaP / 2])}, {(√(pP)) (E^(I * phiP)) (Cos[thetaP / 2])}});
J1D3L = ({{(S1D3L.g0.PL.S2D3L)[[1, 1]]}, {(S1D3L.g1.PL.S2D3L)[[1, 1]]},
    {(S1D3L.g2.PL.S2D3L)[[1, 1]]}, {(S1D3L.g3.PL.S2D3L)[[1, 1]]}});
J2D3L = ({{(S3D3L.g0.Peez.S4D3L)[[1, 1]]}, {(S3D3L.g1.Peez.S4D3L)[[1, 1]]},
    {(S3D3L.g2.Peez.S4D3L)[[1, 1]]}, {(S3D3L.g3.Peez.S4D3L)[[1, 1]]}});
MD3L = (J1D3L^T.MT.J2D3L)[[1, 1]] // Simplify;
MD3LC = MD3L /. {I → -I, -I → I};
MD3L = MD3L * (I * g^2) / (4 * Cos[thetaW]^2 * (mN^2 - 2 * mN * pV - mZ^2)) // Simplify;
MD3LC = MD3LC * (-I * g^2) / (4 * Cos[thetaW]^2 * (mN^2 - 2 * mN * pV - mZ^2)) // Simplify;
```

```
S1D3R = ({{-(√(pV))(Sin[thetaV/2]), (√(pV))(E^(-I*phiV))(Cos[thetaV/2]),
    -(√(pV))(Sin[thetaV/2]), (√(pV))(E^(-I*phiV))(Cos[thetaV/2])}});
S2D3R = ({{0}, {√(2*mN)}, {0}, {0}});
S3D3R = ({{(√(pE))(Cos[thetaE/2]), (√(pE))(E^(-I*phiE))(Sin[thetaE/2]),
    -(√(pE))(Cos[thetaE/2]), -(√(pE))(E^(-I*phiE))(Sin[thetaE/2])}});
S4D3R = ({{(√(pP))(Cos[thetaP/2])}, {(√(pP))(E^(I*phiP))(Sin[thetaP/2])},
   {(√(pP))(Cos[thetaP/2])}, {(√(pP))(E^(I*phiP))(Sin[thetaP/2])}});
J1D3R = ({{(S1D3R.g0.PL.S2D3R)[[1, 1]]}, {(S1D3R.g1.PL.S2D3R)[[1, 1]]},
   {(S1D3R.g2.PL.S2D3R)[[1, 1]]}, {(S1D3R.g3.PL.S2D3R)[[1, 1]]}});
J2D3R = ({{(S3D3R.g0.Peez.S4D3R)[[1, 1]]}, {(S3D3R.g1.Peez.S4D3R)[[1, 1]]},
   {(S3D3R.g2.Peez.S4D3R)[[1, 1]]}, {(S3D3R.g3.Peez.S4D3R)[[1, 1]]}});
MD3R = (J1D3R^T.MT.J2D3R)[[1, 1]] // Simplify;
MD3RC = MD3R /. {I → -I, -I → I};
MD3R = MD3R*(I*g^2)/(4*Cos[thetaW]^2*(mN^2-2*mN*pV-mZ^2)) // Simplify;
MD3RC = MD3RC*(-I*g^2)/(4*Cos[thetaW]^2*(mN^2-2*mN*pV-mZ^2)) // Simplify;
S1D4L = ({{(√(pV))(Cos[thetaV/2]), (√(pV))(E^(-I*phiV))(Sin[thetaV/2]),
    -(√(pV))(Cos[thetaV/2]), -(√(pV))(E^(-I*phiV))(Sin[thetaV/2])}});
S2D4L = ({{√(2*mN)}, {0}, {0}, {0}});
S3D4L = ({{-(√(pE))(Sin[thetaE/2]), (√(pE))(E^(-I*phiE))(Cos[thetaE/2]),
    -(√(pE))(Sin[thetaE/2]), (√(pE))(E^(-I*phiE))(Cos[thetaE/2])}});
S4D4L = ({{(√(pP))(Sin[thetaP/2])}, {-(√(pP))(E^(I*phiP))(Cos[thetaP/2])},
   {-(√(pP))(Sin[thetaP/2])}, {(√(pP))(E^(I*phiP))(Cos[thetaP/2])}});
J1D4L = ({{-(S1D4L.g0.PR.S2D4L)[[1, 1]]}, {-(S1D4L.g1.PR.S2D4L)[[1, 1]]},
   {-(S1D4L.g2.PR.S2D4L)[[1, 1]]}, {-(S1D4L.g3.PR.S2D4L)[[1, 1]]}});
J2D4L = ({{(S3D4L.g0.Peez.S4D4L)[[1, 1]]}, {(S3D4L.g1.Peez.S4D4L)[[1, 1]]},
   {(S3D4L.g2.Peez.S4D4L)[[1, 1]]}, {(S3D4L.g3.Peez.S4D4L)[[1, 1]]}});
MD4L = (J1D4L^T.MT.J2D4L)[[1, 1]] // Simplify;
MD4LC = MD4L /. {I → -I, -I → I};
MD4L = MD4L*(I*g^2)/(4*Cos[thetaW]^2*(mN^2-2*mN*pV-mZ^2)) // Simplify;
MD4LC = MD4LC*(-I*g^2)/(4*Cos[thetaW]^2*(mN^2-2*mN*pV-mZ^2)) // Simplify;
S1D4R = ({{(√(pV))(Cos[thetaV/2]), (√(pV))(E^(-I*phiV))(Sin[thetaV/2]),
    -(√(pV))(Cos[thetaV/2]), -(√(pV))(E^(-I*phiV))(Sin[thetaV/2])}});
S2D4R = ({{√(2*mN)}, {0}, {0}, {0}});
S3D4R = ({{(√(pE))(Cos[thetaE/2]), (√(pE))(E^(-I*phiE))(Sin[thetaE/2]),
    -(√(pE))(Cos[thetaE/2]), -(√(pE))(E^(-I*phiE))(Sin[thetaE/2])}});
S4D4R = ({{(√(pP))(Cos[thetaP/2])}, {(√(pP))(E^(I*phiP))(Sin[thetaP/2])},
   {(√(pP))(Cos[thetaP/2])}, {(√(pP))(E^(I*phiP))(Sin[thetaP/2])}});
J1D4R = ({{-(S1D4R.g0.PR.S2D4R)[[1, 1]]}, {-(S1D4R.g1.PR.S2D4R)[[1, 1]]},
   {-(S1D4R.g2.PR.S2D4R)[[1, 1]]}, {-(S1D4R.g3.PR.S2D4R)[[1, 1]]}});
J2D4R = ({{(S3D4R.g0.Peez.S4D4R)[[1, 1]]}, {(S3D4R.g1.Peez.S4D4R)[[1, 1]]},
   {(S3D4R.g2.Peez.S4D4R)[[1, 1]]}, {(S3D4R.g3.Peez.S4D4R)[[1, 1]]}});
MD4R = (J1D4R^T.MT.J2D4R)[[1, 1]] // Simplify;
MD4RC = MD4R /. {I → -I, -I → I};
MD4R = MD4R*(I*g^2)/(4*Cos[thetaW]^2*(mN^2-2*mN*pV-mZ^2)) // Simplify;
MD4RC = MD4RC*(-I*g^2)/(4*Cos[thetaW]^2*(mN^2-2*mN*pV-mZ^2)) // Simplify;
```

```
S1D5 = ({{0, 0, 0, -√(2 * mN)}});
S2D5 = ({{(√(pP)) (Sin[thetaP / 2])}, {-(√(pP)) (E^(I * phiP)) (Cos[thetaP / 2])},
    {-(√(pP)) (Sin[thetaP / 2])}, {(√(pP)) (E^(I * phiP)) (Cos[thetaP / 2])}});
S3D5 = ({{-(√(pE)) (Sin[thetaE / 2]), (√(pE)) (E^(-I * phiE)) (Cos[thetaE / 2]),
     -(√(pE)) (Sin[thetaE / 2]), (√(pE)) (E^(-I * phiE)) (Cos[thetaE / 2])}});
S4D5 = ({{(√(pV)) (Sin[thetaV / 2])}, {-(√(pV)) (E^(I * phiV)) (Cos[thetaV / 2])},
    {-(√(pV)) (Sin[thetaV / 2])}, {(√(pV)) (E^(I * phiV)) (Cos[thetaV / 2])}});
J1D5 = ({{(S1D5.g0.PL.S2D5)[[1, 1]]}, {(S1D5.g1.PL.S2D5)[[1, 1]]},
    {(S1D5.g2.PL.S2D5)[[1, 1]]}, {(S1D5.g3.PL.S2D5)[[1, 1]]}});
J2D5 = ({{(S3D5.g0.PL.S4D5)[[1, 1]]}, {(S3D5.g1.PL.S4D5)[[1, 1]]},
    {(S3D5.g2.PL.S4D5)[[1, 1]]}, {(S3D5.g3.PL.S4D5)[[1, 1]]}});
MD5 = (J1D5ᵀ.MT.J2D5)[[1, 1]] // Simplify;
MD5C = MD5 /. {I → -I, -I → I};
MD5 = MD5 * (I * g^2) / (2 * (mN^2 - 2 * mN * pP - mW^2)) // Simplify;
MD5C = MD5C * (-I * g^2) / (2 * (mN^2 - 2 * mN * pP - mW^2)) // Simplify;
S1D6 = ({{0, 0, -√(2 * mN), 0}});
S2D6 = ({{(√(pE)) (Cos[thetaE / 2])}, {(√(pE)) (E^(I * phiE)) (Sin[thetaE / 2])},
    {(√(pE)) (Cos[thetaE / 2])}, {(√(pE)) (E^(I * phiE)) (Sin[thetaE / 2])}});
S3D6 = ({{-(√(pV)) (Sin[thetaV / 2]), (√(pV)) (E^(-I * phiV)) (Cos[thetaV / 2]),
     -(√(pV)) (Sin[thetaV / 2]), (√(pV)) (E^(-I * phiV)) (Cos[thetaV / 2])}});
S4D6 = ({{(√(pP)) (Sin[thetaP / 2])}, {-(√(pP)) (E^(I * phiP)) (Cos[thetaP / 2])},
    {-(√(pP)) (Sin[thetaP / 2])}, {(√(pP)) (E^(I * phiP)) (Cos[thetaP / 2])}});
J1D6 = ({{-(S1D6.g0.PR.S2D6)[[1, 1]]}, {-(S1D6.g1.PR.S2D6)[[1, 1]]},
    {-(S1D6.g2.PR.S2D6)[[1, 1]]}, {-(S1D6.g3.PR.S2D6)[[1, 1]]}});
J2D6 = ({{(S3D6.g0.PL.S4D6)[[1, 1]]}, {(S3D6.g1.PL.S4D6)[[1, 1]]},
    {(S3D6.g2.PL.S4D6)[[1, 1]]}, {(S3D6.g3.PL.S4D6)[[1, 1]]}});
MD6 = (J1D6ᵀ.MT.J2D6)[[1, 1]] // Simplify;
MD6C = MD6 /. {I → -I, -I → I};
MD6 = MD6 * (I * g^2) / (2 * (mN^2 - 2 * mN * pE - mW^2)) // Simplify;
MD6C = MD6C * (-I * g^2) / (2 * (mN^2 - 2 * mN * pE - mW^2)) // Simplify;
S1D7 = ({{-(√(pE)) (Sin[thetaE / 2]), (√(pE)) (E^(-I * phiE)) (Cos[thetaE / 2]),
     -(√(pE)) (Sin[thetaE / 2]), (√(pE)) (E^(-I * phiE)) (Cos[thetaE / 2])}});
S2D7 = ({{0}, {√(2 * mN)}, {0}, {0}});
S3D7 = ({{-(√(pV)) (Sin[thetaV / 2]), (√(pV)) (E^(-I * phiV)) (Cos[thetaV / 2]),
     -(√(pV)) (Sin[thetaV / 2]), (√(pV)) (E^(-I * phiV)) (Cos[thetaV / 2])}});
S4D7 = ({{(√(pP)) (Sin[thetaP / 2])}, {-(√(pP)) (E^(I * phiP)) (Cos[thetaP / 2])},
    {-(√(pP)) (Sin[thetaP / 2])}, {(√(pP)) (E^(I * phiP)) (Cos[thetaP / 2])}});
J1D7 = ({{(S1D7.g0.PL.S2D7)[[1, 1]]}, {(S1D7.g1.PL.S2D7)[[1, 1]]},
    {(S1D7.g2.PL.S2D7)[[1, 1]]}, {(S1D7.g3.PL.S2D7)[[1, 1]]}});
J2D7 = ({{(S3D7.g0.PL.S4D7)[[1, 1]]}, {(S3D7.g1.PL.S4D7)[[1, 1]]},
    {(S3D7.g2.PL.S4D7)[[1, 1]]}, {(S3D7.g3.PL.S4D7)[[1, 1]]}});
MD7 = (J1D7ᵀ.MT.J2D7)[[1, 1]] // Simplify;
MD7C = MD7 /. {I → -I, -I → I};
MD7 = MD7 * (I * g^2) / (2 * (mN^2 - 2 * mN * pE - mW^2)) // Simplify;
MD7C = MD7C * (-I * g^2) / (2 * (mN^2 - 2 * mN * pE - mW^2)) // Simplify;
```

```
S1D8 = ({{(√(pP)) (Cos[thetaP / 2]), (√(pP)) (E^(-I * phiP)) (Sin[thetaP / 2]),
      -(√(pP)) (Cos[thetaP / 2]), -(√(pP)) (E^(-I * phiP)) (Sin[thetaP / 2])}});
S2D8 = ({{√(2 * mN)}, {0}, {0}, {0}});
S3D8 = ({{-(√(pE)) (Sin[thetaE / 2]), (√(pE)) (E^(-I * phiE)) (Cos[thetaE / 2]),
      -(√(pE)) (Sin[thetaE / 2]), (√(pE)) (E^(-I * phiE)) (Cos[thetaE / 2])}});
S4D8 = ({{(√(pV)) (Sin[thetaV / 2])}, {-(√(pV)) (E^(I * phiV)) (Cos[thetaV / 2])},
     {-(√(pV)) (Sin[thetaV / 2])}, {(√(pV)) (E^(I * phiV)) (Cos[thetaV / 2])}});
J1D8 = ({{-(S1D8.g0.PR.S2D8)[[1, 1]]}, {-(S1D8.g1.PR.S2D8)[[1, 1]]},
     {-(S1D8.g2.PR.S2D8)[[1, 1]]}, {-(S1D8.g3.PR.S2D8)[[1, 1]]}});
J2D8 = ({{(S3D8.g0.PL.S4D8)[[1, 1]]}, {(S3D8.g1.PL.S4D8)[[1, 1]]},
     {(S3D8.g2.PL.S4D8)[[1, 1]]}, {(S3D8.g3.PL.S4D8)[[1, 1]]}});
MD8 = (J1D8^T.MT.J2D8)[[1, 1]] // Simplify;
MD8C = MD8 /. {I → -I, -I → I};
MD8 = MD8 * (I * g^2) / (2 * (mN^2 - 2 * mN * pP - mW^2)) // Simplify;
MD8C = MD8C * (-I * g^2) / (2 * (mN^2 - 2 * mN * pP - mW^2)) // Simplify;

In[ ]:= T15 = FullSimplify[
    Simplify[ComplexExpand[MD1L * MD1LC]] + Simplify[ComplexExpand[MD1L * MD5C]] +
     Simplify[ComplexExpand[MD5 * MD1LC]] + Simplify[ComplexExpand[MD5 * MD5C]]];
T26 = FullSimplify[
    Simplify[ComplexExpand[MD2L * MD2LC]] + Simplify[ComplexExpand[MD2L * MD6C]] +
     Simplify[ComplexExpand[MD6 * MD2LC]] + Simplify[ComplexExpand[MD6 * MD6C]]];
T37 = FullSimplify[
    Simplify[ComplexExpand[MD3L * MD3LC]] + Simplify[ComplexExpand[MD3L * MD7C]] +
     Simplify[ComplexExpand[MD7 * MD3LC]] + Simplify[ComplexExpand[MD7 * MD7C]]];
T48 = FullSimplify[
    Simplify[ComplexExpand[MD4L * MD4LC]] + Simplify[ComplexExpand[MD4L * MD8C]] +
     Simplify[ComplexExpand[MD8 * MD4LC]] + Simplify[ComplexExpand[MD8 * MD8C]]];
T1 = FullSimplify[ComplexExpand[MD1R * MD1RC]];
T2 = FullSimplify[ComplexExpand[MD2R * MD2RC]];
T3 = FullSimplify[ComplexExpand[MD3R * MD3RC]];
T4 = FullSimplify[ComplexExpand[MD4R * MD4RC]];

In[ ]:= MajAmpSqr = T15 + T26 + T37 + T48 + T1 + T2 + T3 + T4;
DirAmpSqr = T15 + T37 + T1 + T3;

In[ ]:= MajDifDecWid =
  MajAmpSqr * (-((mN^2 Sin[thetaE] Sin[thetaEE] Sin[thetaEV] Sin[thetaEE + thetaEV]) /
        (Sin[thetaEE] + Sin[thetaEV] - Sin[thetaEE + thetaEV])^3)) / ((2 * Pi)^5 * 16 * mN);
DirDifDecWid =
  DirAmpSqr * (-((mN^2 Sin[thetaE] Sin[thetaEE] Sin[thetaEV] Sin[thetaEE + thetaEV]) /
        (Sin[thetaEE] + Sin[thetaEV] - Sin[thetaEE + thetaEV])^3)) / ((2 * Pi)^5 * 16 * mN);

In[ ]:= g = 0.65;
mW = 80.4;
mZ = 91.2;
thetaW = 0.463;
phiE = 0;
```

```
In[ ]:= pV = mN - pE - pP;
        thetaP =
          ArcCos[Sin[thetaE] * Sin[beta] * Sin[thetaEE] + Cos[thetaE] * Cos[thetaEE]] // Simplify;
        phiP = ArcSin[(Cos[beta] * Sin[thetaEE]) / Sin[thetaP]] // Simplify;
        thetaV =
          ArcCos[Cos[thetaE] * Cos[thetaEV] - Sin[thetaE] * Sin[beta] * Sin[thetaEV]] // Simplify;
        phiV = ArcSin[-((Cos[beta] * Sin[thetaEV]) / Sin[thetaV])] // Simplify;
        pE = (-mN * Sin[thetaEE + thetaEV]) / (Sin[thetaEV] + Sin[thetaEE] - Sin[thetaEE + thetaEV]);
        pP = (mN * Sin[thetaEV]) / (Sin[thetaEV] + Sin[thetaEE] - Sin[thetaEE + thetaEV]);

In[ ]:= MajDifDecWid = MajDifDecWid * 2 * Pi;
        DirDifDecWid = DirDifDecWid * 2 * Pi;

In[ ]:= DWM20 = NIntegrate[MajDifDecWid /. mN → 20, {thetaEE, 0, Pi},
            {thetaEV, Pi - thetaEE, Pi}, {beta, 0, 2 * Pi}, {thetaE, 0, Pi}];
        DWM50 = NIntegrate[MajDifDecWid /. mN → 50, {thetaEE, 0, Pi},
            {thetaEV, Pi - thetaEE, Pi}, {beta, 0, 2 * Pi}, {thetaE, 0, Pi}];
        DWM70 = NIntegrate[MajDifDecWid /. mN → 70, {thetaEE, 0, Pi},
            {thetaEV, Pi - thetaEE, Pi}, {beta, 0, 2 * Pi}, {thetaE, 0, Pi}];
        DWD20 = NIntegrate[DirDifDecWid /. mN → 20, {thetaEE, 0, Pi},
            {thetaEV, Pi - thetaEE, Pi}, {beta, 0, 2 * Pi}, {thetaE, 0, Pi}];
        DWD50 = NIntegrate[DirDifDecWid /. mN → 50, {thetaEE, 0, Pi},
            {thetaEV, Pi - thetaEE, Pi}, {beta, 0, 2 * Pi}, {thetaE, 0, Pi}];
        DWD70 = NIntegrate[DirDifDecWid /. mN → 70, {thetaEE, 0, Pi},
            {thetaEV, Pi - thetaEE, Pi}, {beta, 0, 2 * Pi}, {thetaE, 0, Pi}];

In[ ]:= dirac20plot =
         ParametricPlot[{Cos[thetaEE],
          1 / DWD20 * NIntegrate[
           DirDifDecWid /. {mN → 20}, {beta, 0, 2 * Pi}, {thetaE, 0,
            Pi}, {thetaEV, Pi - thetaEE, Pi}]}, {thetaEE, 0, Pi},
         PlotStyle → {Red}, PlotLabel → "20 GeV HNL",
         Frame → {True, True, False, False}, PlotRangePadding → 0, AspectRatio → 0.5,
         FrameLabel → {HoldForm[Cos[Subscript[θ, ee]]],
          HoldForm[(1 / Γ) . ∂_{θ_ee} Γ]},
         Axes → {False, False}, LabelStyle → Black, RotateLabel → False,
         PlotLegends → {"Dirac"}];
        majorana20plot =
         ParametricPlot[{Cos[thetaEE],
          1 / DWM20 * NIntegrate[
           MajDifDecWid /. {mN → 20}, {beta, 0, 2 * Pi}, {thetaE, 0,
            Pi}, {thetaEV, Pi - thetaEE, Pi}]}, {thetaEE, 0, Pi},
         PlotStyle → {Red, Dashed}, PlotLabel → "20 GeV HNL",
         Frame → {True, True, False, False}, PlotRangePadding → 0, AspectRatio → 0.5,
         FrameLabel → {HoldForm[Cos[Subscript[θ, ee]]],
          HoldForm[(1 / Γ) . ∂_{θ_ee} Γ]},
         Axes → {False, False}, LabelStyle → Black, RotateLabel → False,
         PlotLegends → {"Majorana"}];
```

```
dirac50plot =
 ParametricPlot[{Cos[thetaEE],
  1 / DWD50 * NIntegrate[
   DirDifDecWid /. {mN → 50}, {beta, 0, 2 * Pi}, {thetaE, 0,
    Pi}, {thetaEV, Pi - thetaEE, Pi}]}, {thetaEE, 0, Pi},
 PlotStyle → {Blue}, PlotLabel → "50 GeV HNL",
 Frame → {True, True, False, False}, PlotRangePadding → 0, AspectRatio → 0.5,
 FrameLabel → {HoldForm[Cos[Subscript[θ, ee]]],
  HoldForm[ (1 / Γ) . ∂θee Γ]},
 Axes → {False, False}, LabelStyle → Black, RotateLabel → False,
 PlotLegends → {"Dirac"}];
majorana50plot =
 ParametricPlot[{Cos[thetaEE],
  1 / DWM50 * NIntegrate[
   MajDifDecWid /. {mN → 50}, {beta, 0, 2 * Pi}, {thetaE, 0,
    Pi}, {thetaEV, Pi - thetaEE, Pi}]}, {thetaEE, 0, Pi},
 PlotStyle → {Blue, Dashed}, PlotLabel → "50 GeV HNL",
 Frame → {True, True, False, False}, PlotRangePadding → 0, AspectRatio → 0.5,
 FrameLabel → {HoldForm[Cos[Subscript[θ, ee]]],
  HoldForm[(1 / Γ) . ∂θee Γ]},
 Axes → {False, False}, LabelStyle → Black, RotateLabel → False,
 PlotLegends → {"Majorana"}];
```

```
dirac70plot =
 ParametricPlot[{Cos[thetaEE],
  1 / DWD70 * NIntegrate[
   DirDifDecWid /. {mN → 70}, {beta, 0, 2 * Pi}, {thetaE, 0,
    Pi}, {thetaEV, Pi - thetaEE, Pi}]}, {thetaEE, 0, Pi},
 PlotStyle → {Magenta}, PlotLabel → "70 GeV HNL",
 Frame → {True, True, False, False}, PlotRangePadding → 0, AspectRatio → 0.5,
 FrameLabel → {HoldForm[Cos[Subscript[θ, ee]]],
  HoldForm[ (1 / Γ) . ∂θee Γ]},
 Axes → {False, False}, LabelStyle → Black, RotateLabel → False,
 PlotLegends → {"Dirac"}];
majorana70plot =
 ParametricPlot[{Cos[thetaEE],
  1 / DWM70 * NIntegrate[
   MajDifDecWid /. {mN → 70}, {beta, 0, 2 * Pi}, {thetaE, 0,
    Pi}, {thetaEV, Pi - thetaEE, Pi}]}, {thetaEE, 0, Pi},
 PlotStyle → {Magenta, Dashed}, PlotLabel → "70 GeV HNL",
 Frame → {True, True, False, False}, PlotRangePadding → 0, AspectRatio → 0.5,
 FrameLabel → {HoldForm[Cos[Subscript[θ, ee]]],
  HoldForm[(1 / Γ) . ∂θee Γ]},
 Axes → {False, False}, LabelStyle → Black, RotateLabel → False,
 PlotLegends → {"Majorana"}];
```

In[ ]:=
```
plot20gev = Show[dirac20plot, majorana20plot]
plot50gev = Show[dirac50plot, majorana50plot]
plot70gev = Show[dirac70plot, majorana70plot]
```

Out[ ]=

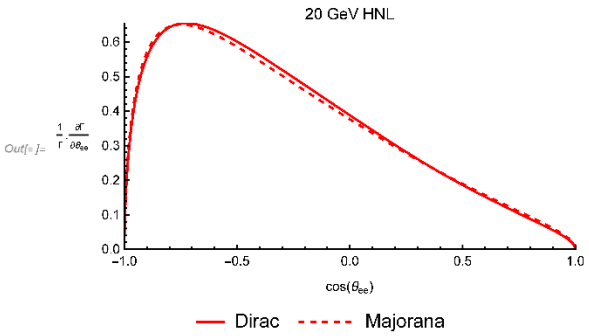

Out[ ]=

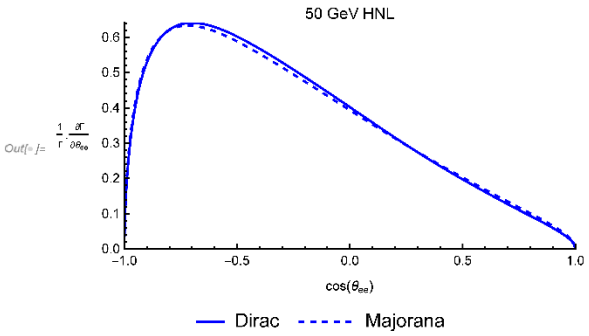

Out[ ]=

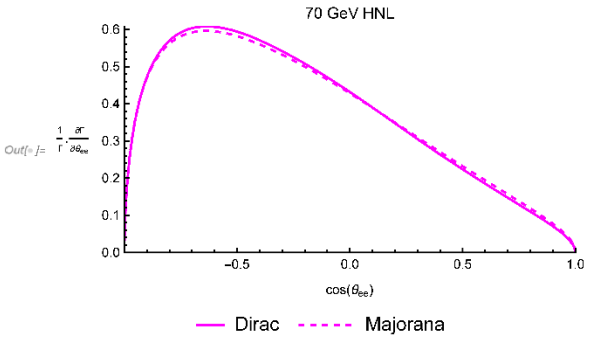

```
mtm20plot = Plot[1, {x, -1, 1}, PlotStyle → {Red, Dashed},
 Frame → {True, True, False, False}, PlotRangePadding → 0, AspectRatio → 0.25,
 FrameLabel → {HoldForm[Cos[Subscript[θ, ee]]],
  HoldForm["Dirac/Majorana Ratio"]},
 Axes → {False, False}, LabelStyle → Black, RotateLabel → False,
 PlotLegends → {"Majorana"}];
dtm20plot = ParametricPlot[{Cos[thetaEE],
  (1 / DWD20 * NIntegrate[
   DirDifDecWid /. {mN → 20}, {beta, 0, 2 * Pi}, {thetaE, 0,
    Pi}, {thetaEV, Pi - thetaEE, Pi}]) / (1 / DWM20 * NIntegrate[
   MajDifDecWid /. {mN → 20}, {beta, 0, 2 * Pi}, {thetaE, 0,
    Pi}, {thetaEV, Pi - thetaEE, Pi}])}, {thetaEE, 0, Pi},
 PlotStyle → {Red},
 Frame → {True, True, False, False}, PlotRangePadding → 0, AspectRatio → 0.25,
 FrameLabel → {HoldForm[Cos[Subscript[θ, ee]]],
  HoldForm["Dirac/Majorana Ratio"]},
 Axes → {False, False}, LabelStyle → Black, RotateLabel → False,
 PlotLegends → {"Dirac"}];
```

```
mtm50plot = Plot[1, {x, -1, 1}, PlotStyle → {Blue, Dashed},
 Frame → {True, True, False, False}, PlotRangePadding → 0, AspectRatio → 0.25,
 FrameLabel → {HoldForm[Cos[Subscript[θ, ee]]],
  HoldForm["Dirac/Majorana Ratio"]},
 Axes → {False, False}, LabelStyle → Black, RotateLabel → False,
 PlotLegends → {"Majorana"}];
dtm50plot = ParametricPlot[{Cos[thetaEE],
  (1 / DWD50 * NIntegrate[
   DirDifDecWid /. {mN → 50}, {beta, 0, 2 * Pi}, {thetaE, 0,
    Pi}, {thetaEV, Pi - thetaEE, Pi}]) / (1 / DWM50 * NIntegrate[
   MajDifDecWid /. {mN → 50}, {beta, 0, 2 * Pi}, {thetaE, 0,
    Pi}, {thetaEV, Pi - thetaEE, Pi}])}, {thetaEE, 0, Pi},
 PlotStyle → {Blue},
 Frame → {True, True, False, False}, PlotRangePadding → 0, AspectRatio → 0.25,
 FrameLabel → {HoldForm[Cos[Subscript[θ, ee]]],
  HoldForm["Dirac/Majorana Ratio"]},
 Axes → {False, False}, LabelStyle → Black, RotateLabel → False,
 PlotLegends → {"Dirac"}];
```

```
In[•]:= mtm70plot = Plot[1, {x, -1, 1}, PlotStyle → {Magenta, Dashed},
         Frame → {True, True, False, False}, PlotRangePadding → 0, AspectRatio → 0.25,
         FrameLabel → {HoldForm[Cos[Subscript[θ, ee]]],
          HoldForm["Dirac/Majorana Ratio"]},
         Axes → {False, False}, LabelStyle → Black, RotateLabel → False,
         PlotLegends → {"Majorana"}];
        dtm70plot = ParametricPlot[{Cos[thetaEE],
          (1 / DWD70 * NIntegrate[
           DirDifDecWid /. {mN → 70}, {beta, 0, 2 * Pi}, {thetaE, 0,
            Pi}, {thetaEV, Pi - thetaEE, Pi}]) / (1 / DWM70 * NIntegrate[
           MajDifDecWid /. {mN → 70}, {beta, 0, 2 * Pi}, {thetaE, 0,
            Pi}, {thetaEV, Pi - thetaEE, Pi}])}, {thetaEE, 0, Pi},
         PlotStyle → {Magenta},
         Frame → {True, True, False, False}, PlotRangePadding → 0, AspectRatio → 0.25,
         FrameLabel → {HoldForm[Cos[Subscript[θ, ee]]],
          HoldForm["Dirac/Majorana Ratio"]},
         Axes → {False, False}, LabelStyle → Black, RotateLabel → False,
         PlotLegends → {"Dirac"}];

In[•]:= ratioplot20gev = Show[dtm20plot, mtm20plot]
        ratioplot50gev = Show[dtm50plot, mtm50plot]
        ratioplot70gev = Show[dtm70plot, mtm70plot]
```

Out[•]=

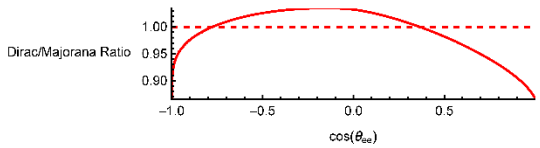

Out[•]=

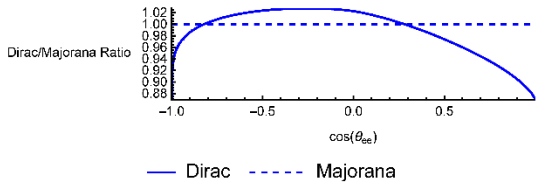

Out[•]=

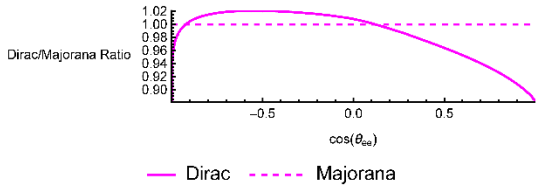

Appendix B

It was initially planned for this section to provide a thorough and detailed explanation for the process of sample generation and sample analysis that was done for the experimental part of the project. However, as the analysis was conducted within the FCC framework, which is an evolving framework, it would be better for the reader to look at the explanations of the processes at the appropriate repositories. In the starting days of this project being undertaken, many scripts had to be written to perform the full analysis chain, however, during the time of writing of this thesis, many scripts that achieve such objectives are now provided in a standardized way in the FCC repositories. In particular,

- The FCC repository is available at: https://github.com/HEP-FCC
- The FCC Analysis repository is available at: https://github.com/HEP-FCC/FCCAnalyses
- The FCC-ee Long Lived Particles repository is available at: https://github.com/HEP-FCC/FCCeePhysicsPerformance/tree/master/case-studies/BSM/LLP
- The HNL model files for Madgraph event generation are available at: https://feynrules.irmp.ucl.ac.be/wiki/HeavyN

The entire experimental simulations and analysis were performed on CERN's lxplus system.

References

1. Hernandez, P. "Neutrino Physics." *Proceedings of the 2015 CERN-Latin-American School of High-Energy Physics*, August 3, 2017. https://doi.org/10.5170/CERN-2016-005.85.
2. Wu, C. S., E. Ambler, R. W. Hayward, D. D. Hoppes, and R. P. Hudson. "Experimental Test of Parity Conservation in Beta Decay." *Physical Review* 105, no. 4 (1957): 1413–15. https://doi.org/10.1103/physrev.105.1413.
3. Lesgourgues, Julien, Sergio Pastor, Gennaro Miele, and Gianpiero Mangano. *Neutrino Cosmology*. Cambridge: Cambridge University Press, 2013.
4. Atre, Anupama, Tao Han, Silvia Pascoli, and Bin Zhang. "The Search for Heavy Majorana Neutrinos." *Journal of High Energy Physics* 2009, no. 05 (2009). https://doi.org/10.1088/1126-6708/2009/05/030.
5. Pascoli, Silvia, Richard Ruiz, and Cedric Weiland. "Heavy Neutrinos with Dynamic Jet Vetoes: Multilepton Searches at $$ \Sqrt{s}=14 $$, 27, and 100 TEV." *Journal of High Energy Physics* 2019, no. 6 (2019). https://doi.org/10.1007/jhep06(2019)049.
6. Denner, A., H. Eck, O. Hahn, and J. Küblbeck. "Feynman Rules for Fermion-Number-Violating Interactions." *Nuclear Physics B* 387, no. 2 (1992): 467–81. https://doi.org/10.1016/0550-3213(92)90169-c.
7. Ruiz, Richard. "Quantitative Study on Helicity Inversion in Majorana Neutrino Decays at the LHC." *Physical Review D* 103, no. 1 (2021). https://doi.org/10.1103/physrevd.103.015022.
8. Zyla, P, et al. "Review of Particle Physics." *Progress of Theoretical and Experimental Physics* 2020, no. 8 (2020). https://doi.org/10.1093/ptep/ptaa104.
9. Abada, A., et al. "FCC-ee: The Lepton Collider." *The European Physical Journal Special Topics*, June 4, 2019, 261–623. https://doi.org/https://doi.org/10.1140/epjst/e2019-900045-4.
10. Stelzer, T., and W.F. Long. "Automatic Generation of Tree Level Helicity Amplitudes." *Computer Physics Communications* 81, no. 3 (1994): 357–71. https://doi.org/10.1016/0010-4655(94)90084-1.

11. Alwall, J., R. Frederix, S. Frixione, V. Hirschi, F. Maltoni, O. Mattelaer, H.-S. Shao, T. Stelzer, P. Torrielli, and M. Zaro. "The Automated Computation of Tree-Level and next-to-Leading Order Differential Cross Sections, and Their Matching to Parton Shower Simulations." *Journal of High Energy Physics* 2014, no. 7 (2014). https://doi.org/10.1007/jhep07(2014)079.
12. Sjöstrand, Torbjörn, Stefan Ask, Jesper R. Christiansen, Richard Corke, Nishita Desai, Philip Ilten, Stephen Mrenna, Stefan Prestel, Christine O. Rasmussen, and Peter Z. Skands. "An Introduction to Pythia 8.2." *Computer Physics Communications* 191 (2015): 159–77. https://doi.org/10.1016/j.cpc.2015.01.024.
13. Alva, Daniel, Tao Han, and Richard Ruiz. "Heavy Majorana Neutrinos from Wγ Fusion at Hadron Colliders." *Journal of High Energy Physics* 2015, no. 2 (2015). https://doi.org/10.1007/jhep02(2015)072.
14. Degrande, Céline, Olivier Mattelaer, Richard Ruiz, and Jessica Turner. "Fully Automated Precision Predictions for Heavy Neutrino Production Mechanisms at Hadron Colliders." *Physical Review D* 94, no. 5 (2016). https://doi.org/10.1103/physrevd.94.053002.
15. de Favereau, J., C. Delaere, P. Demin, A. Giammanco, V. Lemaître, A. Mertens, and M. Selvaggi. "DELPHES 3: A Modular Framework for Fast Simulation of a Generic Collider Experiment." *Journal of High Energy Physics* 2014, no. 2 (2014). https://doi.org/10.1007/jhep02(2014)057.
16. RD-FA Collaboration, and M Antonello. "IDEA: A Detector Concept for Future Leptonic Colliders." *IL NUOVO CIMENTO C*, October 20, 2020. https://doi.org/10.1393/ncc/i2020-20027-2.
17. Alimena, J., et al. "Searches for Long-Lived Particles at the Future FCC-ee," *arXiv:2203.05502*, March 2022. https://doi.org/arXiv:2203.05502.
18. Kayser, Boris. "Majorana Neutrinos and Their Electromagnetic Properties." *Physical Review D* 26, no. 7 (1982): 1662–70. https://doi.org/10.1103/physrevd.26.1662.